

Rational Design of Indoleamine 2,3-Dioxygenase Inhibitors

Ute F. Röhrig,^{†,*,○} Loay Awad,^{†,§,○} Aurélien Grosdidier,[‡] Pierre Larrieu,^{||,⊥} Vincent Stroobant,^{||,⊥} Didier Colau,^{||,⊥} Vincenzo Cerundolo,[▽] Andrew J. G. Simpson,[#] Pierre Vogel,[§] Benoît J. Van den Eynde,^{||,⊥} Vincent Zoete,^{*,‡} and Olivier Michielin^{*,†,‡,⊙}

[†]Ludwig Institute for Cancer Research, Lausanne Branch, CH-1015 Lausanne, Switzerland, [‡]Swiss Institute of Bioinformatics, Molecular Modeling Group, CH-1015 Lausanne, Switzerland, [§]Laboratory of Glycochemistry and Asymmetric Synthesis, Ecole Polytechnique Fédérale de Lausanne (EPFL), CH-1015 Lausanne, Switzerland, ^{||}Cellular Genetics Unit, Institute of Cellular Pathology, Université Catholique de Louvain, B-1200 Brussels, Belgium, [⊥]Ludwig Institute for Cancer Research, Brussels Branch, B-1200 Brussels, Belgium, [▽]Tumour Immunology Group, Weatherall Institute of Molecular Medicine, John Radcliffe Hospital, Oxford, United Kingdom, [#]Ludwig Institute for Cancer Research, Memorial Sloan-Kettering Cancer Center, New York, New York 10158, and [⊙]Pluridisciplinary Centre for Clinical Oncology (CePO), Centre Hospitalier Universitaire Vaudois (CHUV), Lausanne, Switzerland. [○]Both authors contributed equally to this work.

Received October 5, 2009

Indoleamine 2,3-dioxygenase (IDO) is an important therapeutic target for the treatment of diseases such as cancer that involve pathological immune escape. We have used the evolutionary docking algorithm EADock to design new inhibitors of this enzyme. First, we investigated the modes of binding of all known IDO inhibitors. On the basis of the observed docked conformations, we developed a pharmacophore model, which was then used to devise new compounds to be tested for IDO inhibition. We also used a fragment-based approach to design and to optimize small organic molecule inhibitors. Both approaches yielded several new low-molecular weight inhibitor scaffolds, the most active being of nanomolar potency in an enzymatic assay. Cellular assays confirmed the potential biological relevance of four different scaffolds.

Introduction

Many tumors develop the capacity to actively suppress a potentially effective immune response. A growing body of evidence implicates the involvement of the enzyme indoleamine 2,3-dioxygenase (IDO,^a EC 1.13.11.52) in this pathological immune escape, suggesting IDO as a therapeutic target for pharmacological interventions.^{1–3}

IDO catalyzes the initial, and rate-limiting, step in the catabolism of tryptophan (Trp) along the kynurenine pathway.^{4,5} By depleting Trp locally, IDO blocks the proliferation of T lymphocytes, which are sensitive to Trp shortage.⁶ The observations that many human tumors constitutively express IDO⁷ and that an increased level of IDO expression in tumor cells is correlated with poor prognosis for survival in several cancer types^{8–11} led to the hypothesis that its inhibition might enhance the efficacy of cancer treatments. Indeed, results from in vitro and in vivo studies have suggested that the efficacy of therapeutic vaccination or chemotherapy may be improved by concomitant administration of an IDO inhibitor.^{7,12}

IDO is an extrahepatic heme-containing enzyme that displays less substrate specificity than the functionally related enzyme tryptophan 2,3-dioxygenase (TDO).⁵ IDO degrades indoleamines such as L-Trp, D-Trp, serotonin, and tryptamine.¹³ In the first step of the catalytic cycle, IDO binds both

the substrate and molecular oxygen in the distal heme site. The enzyme catalyzes the cleavage of the pyrrole ring of the substrate and incorporates both oxygen atoms before releasing *N*-formylkynurenine, which is subsequently hydrolyzed to kynurenine by cytosolic formamidase. The first crystal structures of IDO reported in 2006 included the heme-bound ligands cyanide and 4-phenylimidazole (PIM).¹⁴ Mutant analyses showed that none of the polar amino acid residues in the distal heme site are essential for the activity of the enzyme, suggesting a reaction mechanism involving only the substrate and the dioxygen molecule.^{14–16} In the active form of IDO, the heme iron is in its ferrous state (Fe²⁺), while in its inactive form, the heme iron is in the ferric (Fe³⁺) state. The catalytic cycle of IDO does not alter the oxidation state of the iron. However, IDO is prone to autoxidation, and therefore, a reductant is necessary in the enzymatic assay to maintain enzyme activity. Cytochrome *b*₅ has been suggested to be responsible for IDO reduction in vivo.^{17,18}

Until a few years ago, the best known IDO inhibitors displayed affinities in the micromolar range and comprised mainly Trp derivatives and β -carbolines.^{5,12,19–25} In 2006, potent nanomolar inhibitors were isolated from marine invertebrate extracts.^{26–28} However, three of the most active compounds were inactive in a yeast-based cellular assay,²⁹ suggesting that they cannot cross the cell membrane. Using the same assay, a screen of the NCI Diversity Set library,³⁰ and of crude natural extracts, yielded 10 active compounds, the best having a *K*_i of 1.5 μ M.²⁹ Around the same time, new brassinin-based IDO inhibitors were published, the best having a *K*_i of 12 μ M³¹ but not being Lipinski-compliant due to high hydrophobicity. In 2008, two new classes of compounds

*To whom correspondence should be addressed. Phone: +41216924053. Fax: +41216924065. E-mail: vincent.zoete@isb-sib.ch or olivier.michielin@isb-sib.ch.

^aAbbreviations: IDO, indoleamine 2,3-dioxygenase; DFT, density functional theory; FBDD, fragment-based drug design; 1MT, 1-methyl-tryptophan; MMBP, Morse-like metal binding potential; PIM, 4-phenylimidazole; rmsd, root-mean-square deviation.

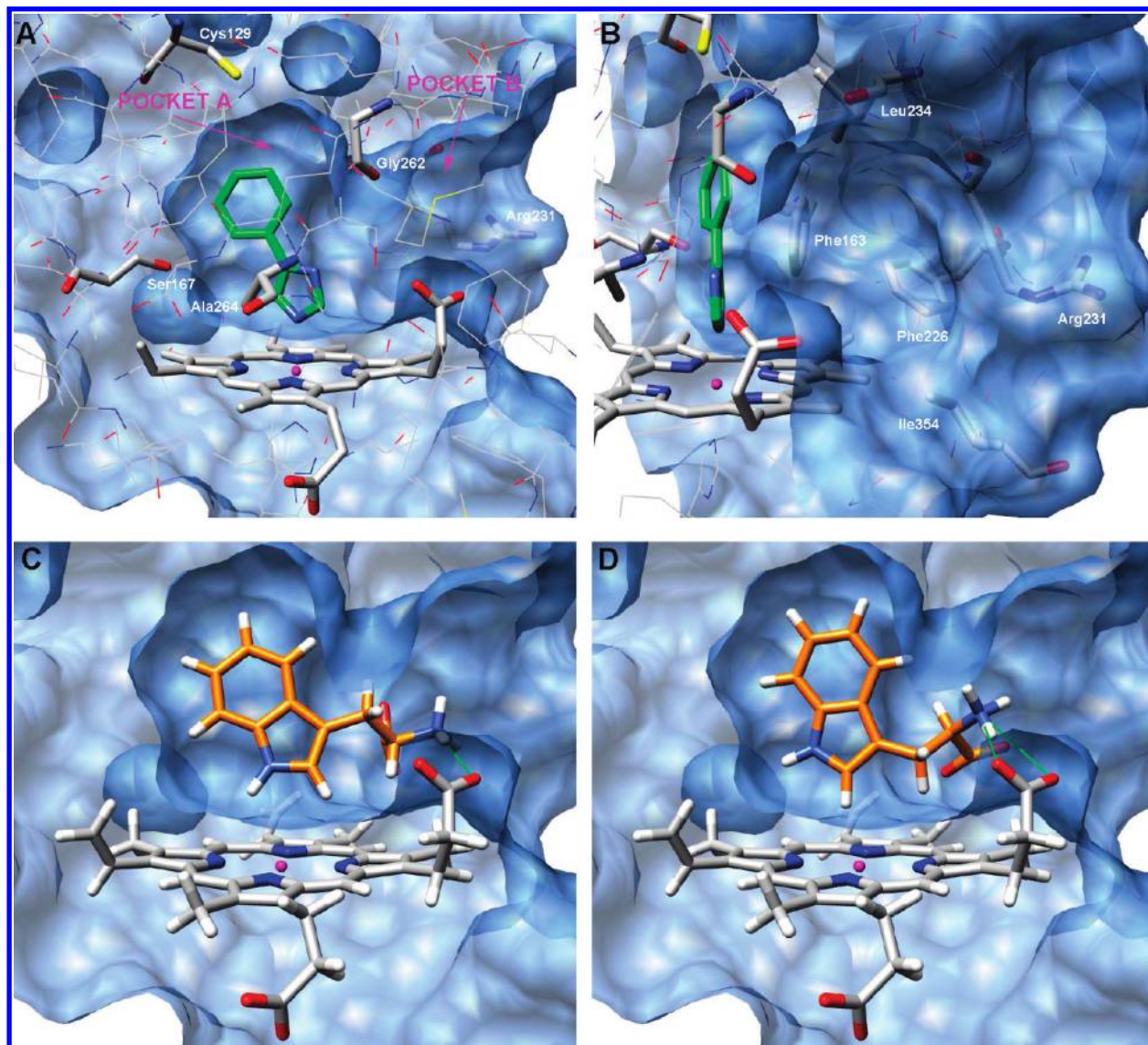


Figure 1. (A and B) X-ray structure of IDO, showing the binding site with the PIM ligand (green). (A) Two hydrophobic pockets and residues within hydrogen bonding distance are labeled. (B) Side view, highlighting the residues that form pocket B. (C) Proposed binding mode for L-Trp (orange). (D) Proposed binding mode for D-Trp (orange).

were reported that were based on the earlier discovery of the marine invertebrate inhibitors. Carr et al. identified tryptamine quinone as the core pharmacophore of exiguamine A²⁷ and described a series of derivatives, the best showing a K_i of 200 nM.^{32,33} Kumar et al. concentrated on the naphthoquinone core of annulin B²⁸ and designed derivatives, partly based on structural modeling, with IC_{50} values of up to 60 nM.³⁴ In parallel to these developments, a structure-based study of PIM-derived molecules led to the discovery of inhibitors with low micromolar activities, a gain of a factor of 10 compared to that of the parent compound.³⁵ A further study designed 1-methyltryptophan (1MT) hybrids as hypoxia-targeting IDO inhibitors.³⁶ Very recently, new natural product inhibitors³⁷ ($IC \approx 2 \mu M$) and potent competitive inhibitors including a hydroxyamidine motif^{38,39} (IC_{50} values of up to 60 nM) have also been described.

A clinical trial is currently investigating the efficacy of 1MT in the treatment of advanced malignancies.² 1MT has long been known to be a competitive IDO inhibitor,²² but there remains a discussion concerning the efficacy of the two stereoisomers. L-1MT inhibits the IDO in a cell-free assay

with a K_i of 19 μM , while D-1MT is inactive.⁴⁰ However, in vivo the D-isomer has been reported to be more efficacious as an anticancer agent in chemo-immunotherapy regimens.⁴⁰ The reason for this discrepancy is still being vigorously debated.^{41–44} Many IDO inhibitors show either noncompetitive or uncompetitive inhibition kinetics similar to those of PIM and norharman,^{20,21} which have been shown to bind directly to the heme iron^{14,21} and to occupy the presumed Trp binding site. The interpretation of IDO inhibition kinetics may, however, be complicated due to the preferential binding of some inhibitors to the inactive ferric form of IDO, and the redox activity of other inhibitors. Since many of the IDO inhibitors that have been discovered recently^{27–29,31,33–37,39} might fail in vivo testing, there is still considerable interest in discovering new IDO inhibitor families.

The two crystal structures of human IDO¹⁴ open the way for the in silico design of new IDO inhibitors. In the PIM-bound X-ray structure [Protein Data Bank (PDB) entry 2D0T], the ligand is bound in a deep binding site with its phenyl ring inside a hydrophobic pocket [pocket A (Figure 1)] and one imidazole nitrogen coordinated to the heme iron at a

distance of 2.1 Å. The PIM binding site consists of residues Tyr126, Cys129, Val130, Phe163, Phe164, Ser167, Leu234, Gly262, Ser263, Ala264, and the heme ring. Possible hydrogen bonding sites are the thiol group of Cys129, the hydroxy group of Ser167, the CO group of Gly262, the NH group of Ala264, and the heme 7-propionate group. Ligands larger than PIM may also interact with Phe226, Arg231, Ser235, Phe291, Ile354, and Leu384, which are located at the binding site entrance. Here, additional hydrogen bonds are possible with the side chain of Arg231. A hydrophobic pocket in this region is provided by Phe163, Phe226, Arg231, Leu234, Ile354, and the heme ring [pocket B (Figure 1)]. The cyanide-bound structure (PDB entry 2D0U) differs from the PIM-bound structure mainly in the access to pocket A, which is hindered by an inward movement of the backbone of the loop of residues 262–266 and the side chain of Phe163, suggesting some flexibility in the active site. In both structures, two buffer molecules are bound at the entrance of the active site, forming a hydrogen bond to the heme propionate and interacting with pocket B.

The aim of this work was to discover novel IDO inhibitors by in silico drug design, using our docking algorithm EA-Dock.^{45,46} We have utilized two approaches. In the first, we investigated the binding modes of all known IDO inhibitors. On the basis of the observed docked conformations, we then developed a pharmacophore model, which was used to devise new compounds to be tested for IDO inhibition. In addition, the pharmacophore model and results from fragment-based screening were also used to select FDA-approved compounds from the Distributed Structure-Searchable Toxicity (DSSTox) database⁴⁷ for docking and screening. In a second approach, we undertook a fragment-based design of small organic molecule inhibitors. Fragment-based drug design (FBDD) has become an established technique both in experimental and in in silico approaches.^{48–51} Its advantages over high-throughput screening include a more complete sampling of chemical space and a better starting point for lead optimization. In addition, the small size of fragment hits results in a high proportion of atoms being directly involved in protein binding, providing a high ligand efficiency.⁵² Optimization thus has a better probability of leading to more efficient and therefore smaller drugs, with better chances of favorable pharmacokinetic properties.⁵³

We used a small library of approximately 60 “molecular frameworks” and “side chains” that were extracted from common features of commercially available drugs.^{54,55} After creating maps of favorable positions for each of these fragments in the IDO active site, we used a fragment linking approach to create new compounds in situ, which were again subjected to the docking procedure to check if they adopt the intended binding mode and exhibit favorable interactions. Fragment-based lead optimization was also applied to active molecules obtained from the pharmacophore-based approach.

Using both approaches, our aim was to design either commercially available or easily synthesizable molecules, to be able to quickly test putative ligands. Commercial compounds were generally identified through the ZINC database and search engine.⁵⁶ Here, we describe the in silico discovery of several novel families of IDO inhibitors, the best having an IC₅₀ in the nanomolar range. Compounds were tested in an enzymatic assay for IDO inhibitory activity, and successful candidates were subsequently tested in a cellular assay. Counterscreening against TDO determined their selectivity for IDO.

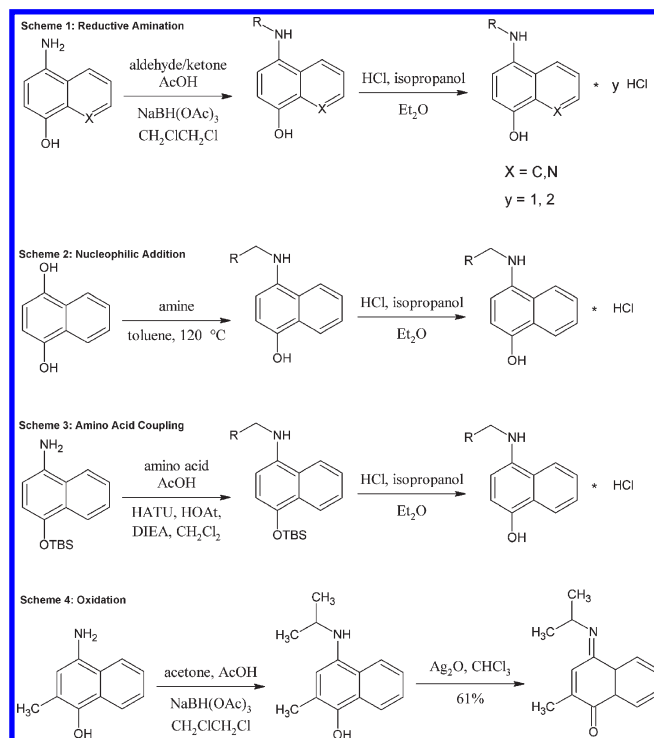


Figure 2. Reaction schemes.

Chemistry

The commercially available hydrochloric salts of 4-amino-1-naphthol and of 5-amino-8-hydroxyquinoline were used to synthesize 4-aminoalkyl-1-naphthol and 5-aminoalkyl-8-hydroxyquinoline derivatives (**31**, **32**, **34–36**, **39**, and **40**) through reductive amination using NaBH(OAc)₃ as the reducing agent⁵⁷ (Scheme 1, Figure 2). We found that the reductive amination can be applied without protection of the hydroxyl group. Hydrochloric salt forms of the amines were prepared for better solubility by dissolving the compounds in dry diethyl ether followed by slow addition of dry hydrochloric acid in 2-propanol or dioxane.

Other 4-aminoalkyl-1-naphthol derivatives (**38** and **41–44**) were, for the first time, prepared by nucleophilic addition (Scheme 2, Figure 2). *p*-Naphthohydroquinone and a small excess of primary amine were refluxed for 1 h in toluene, and the product was obtained by filtration on silica gel.

Some amide analogues of 4-amino-1-naphthol (**46–50**) were prepared by amino acid coupling using a HOAt/HATU mixture (Scheme 3, Figure 2),^{58–61} while compound **51** was prepared via treatment of 1,4-naphthoquinone with ethylene glycol at 120 °C.

The attempt to oxidize 4-aminoalkyl-1-naphthol using Ag₂O or other oxidizing conditions⁶² did not yield the desired 4-(alkylimino)naphthalen-1-one. Degradation products of **34** and oxidized dimers of **36** and **39** (**53** and **54**, respectively) were obtained. We therefore protected 4-amino-1-naphthol in position 2 with a methyl group to prevent dimerization. The reductive amination procedure was applied to 4-amino-2-methyl-1-naphthol (vitamin K5)⁶³ and acetone, followed by oxidation to yield the desired oxidized monomer (**55**, Scheme 4, Figure 2).

Aryl-substituted triazoles (**15–17**) were synthesized according to the method developed by Fokin and co-workers.⁶⁴ Other compounds were synthesized according to literature procedures (**11**,⁶⁵ **14**,⁶⁶ **33**,⁶⁷ **37**,⁶⁸ **45**,⁶⁹ and **52**^{70–72}) or were commercially available (**1–10**, **12**, **13**, **18–30**, and **51**).

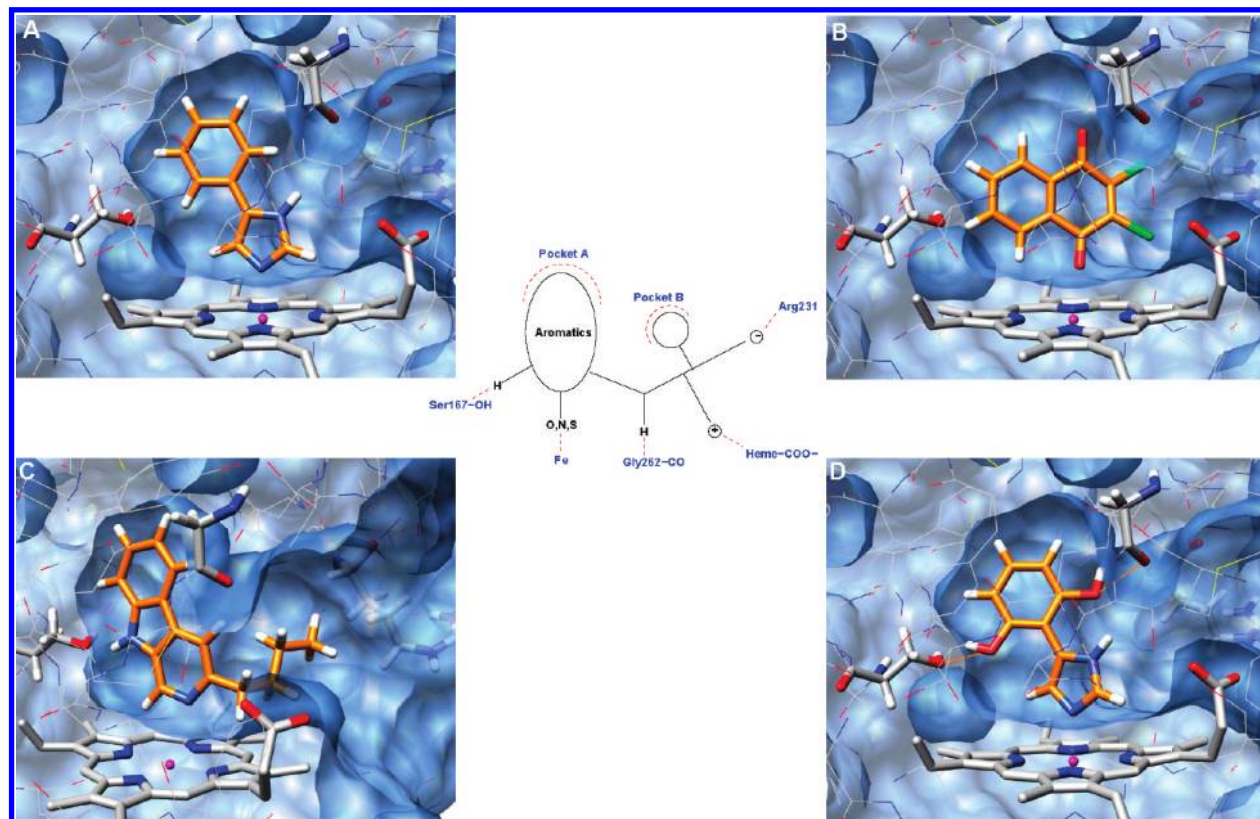


Figure 3. Suggestions for a pharmacophore from docking of known IDO inhibitors. Some important features are displayed around the pharmacophore: (A) an aromatic fragment of at least two rings filling pocket A (PIM), (B) an iron-coordinating atom (2,3-dichloro-1,4-naphthoquinone),³⁴ (C) a hydrophobic group filling pocket B (3-butyl- β -carboline),²³ and (D) groups that can hydrogen bond, e.g., to Ser167 and to Gly262 [2-(imidazol-4-yl)benzene-1,3-diol].³⁵

Results and Discussion

Lead Design from a Pharmacophore Model. As a first test of our docking algorithm,^{45,46} we docked PIM to the IDO active site and observed a good agreement with the X-ray structure (rmsd of 0.3 Å). Application of a Morse-like metal binding potential (MMBP)⁷³ is necessary to reproduce the iron–nitrogen bond of 2.1 Å and improves the rmsd to the X-ray structure by 0.4 Å (Figure 3A).

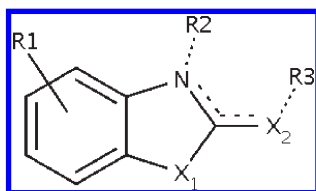
We went on to dock most of the known IDO inhibitors, a total of 134 molecules with an enzymatic K_i or IC_{50} of < 2 mM. These include Trp derivatives and β -carbolines,^{5,12,19,21–24} dithiocarbamates,³¹ naphthoquinones,^{26,28,34} tryptamine quinones,^{27,32,33} *N*-hydroxy-1,2,5-oxadiazole-3-carboximidamides,³⁸ and PIM derivatives.³⁵ Ninety-eight of these biologically active compounds (73%) could be docked successfully according to the criteria described in Docking. The coordinates of all 134 docked compounds are given in the Supporting Information.

Some of the known inhibitors are too large to enter into the binding pocket as provided by the X-ray structure of PIM-bound IDO, especially some of the large quinone compounds^{27,28,33,34} as well as most of the substituted β -carbolines.²³ This suggests that they either bind in a different region of IDO or that the binding pocket is able to adapt to this different class of ligands. In this context, it should be remembered that PIM also does not fit into the binding site of the cyanide-bound X-ray structure of IDO,¹⁴ suggesting some flexibility of the active site.

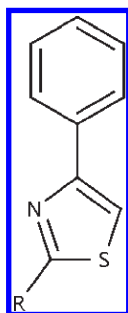
In general, Trp derivatives were found to dock like Trp itself into the IDO active site (Figure 1C,D): the indole ring is

placed in pocket A, with the amino acid pointing toward the entrance of the active site and the positively charged amino group interacting with the heme propionate. L- and D-enantiomers did not exhibit large structural differences. Some of the active β -carbolines (Figure 3C) docked as expected like PIM, filling pocket A with the three aromatic cycles, binding to the heme iron with the pyridine nitrogen, and pointing potential substituents toward the entrance of the active site and pocket B. For the dithiocarbamates, the indole or indole-like aromatic ring was generally found in pocket A, with the dithiocarbamate moiety being located in pocket B. A binding mode involving the sp^2 -hybridized sulfur atom binding to the heme iron as suggested in the original article³¹ was not found. Those of the quinone compounds^{26–28,32–34} that were able to enter pocket A generally indicate a coordination of a quinone oxygen to the heme iron, as suggested previously (Figure 3B).³⁴ The PIM analogues and derivatives studied in ref 35 were mostly found to dock like PIM to IDO, with the two aromatic rings in pocket A and one imidazole nitrogen coordinated to the heme iron (Figure 3A,D). Some compounds with lower activities could not adopt this binding mode. The *N*-hydroxy-1,2,5-oxadiazole-3-carboximidamides³⁸ were found to dock with an oxadiazole nitrogen bound to the heme iron and the other aromatic ring located in pocket B. However, also these ligands could necessitate an adaptation of the active site to be able to place their aromatic ring in pocket A.

On the basis of the observed geometries of the docked ligands, we concluded that a good ligand should contain some or all of the following features (Figure 3): (i) an aromatic fragment, at least bicyclic, to fill pocket A in the

Table 1. Enzymatic Activity of Benzothiazoles

| | X ₁ | X ₂ | R ₁ | R ₂ | R ₃ | IC ₅₀ (μM) |
|-----------|-----------------|----------------|-------------------|-----------------|--|-----------------------|
| 1 | S | S | — | H | — | 50 |
| 2 | S | S | 5-Cl | H | — | 50 |
| 3 | S | S | 6-NH ₂ | H | — | NI ^a |
| 4 | S | NH | — | H | — | NI ^a |
| 5 | NH | S | — | H | — | NI ^a |
| 6 | S | O | — | H | — | NI ^a |
| 7 | NH | O | — | H | — | NI ^a |
| 8 | CH ₂ | O | — | H | — | NI ^a |
| 9 | S | S | — | CH ₃ | — | NI ^a |
| 10 | S | S | — | — | CH ₃ | NI ^a |
| 11 | S | S | — | — | CH ₂ N(CH ₃) ₂ | 50 |

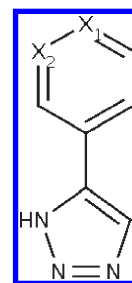
^a No detectable IDO inhibition.**Table 2.** Enzymatic Activity of Phenylthiazoles

| | R | IC ₅₀ (μM) |
|-----------|---|-----------------------|
| 12 | SH | 50 |
| 13 | NH ₂ | 1000 |
| 14 | SCH ₂ N(CH ₃) ₂ | > 1000 |

binding site; (ii) an atom with a free electron pair that can coordinate to the heme iron, such as oxygen, nitrogen, or sulfur; (iii) a group that can form van der Waals interactions with pocket B; and (iv) groups that can hydrogen bond to Ser167, Gly262, Ala264, and Arg231 (possibly a negatively charged group that can form a salt bridge) or to the heme 7-propionate (possibly a positively charged group that can form a salt bridge).

Almost all known IDO inhibitors comply with rule (i). The Trp derivatives and the dithiocarbamates³¹ do not obey rule (ii) but generally show low activities in the higher micromolar range. Rules (iii) and (iv) are commonly observed in larger ligands.

We then used the pharmacophore model to devise new putative IDO ligands. Approximately 50 compounds were docked in silico, and on the basis of their successful docking, a selection of 12 compounds was purchased or synthesized to be tested in the enzymatic assay. This approach yielded three families of active compounds, benzothiazoles, phenylthiazoles, and triazoles (Tables 1–3 and Figure 4A–F). The first is a bioisostere of the indole ring of Trp, while the latter two are bioisosteres of PIM. Successful dockings were defined

Table 3. Enzymatic Activity of Triazoles

| | X ₁ | X ₂ | IC ₅₀ (μM) |
|-----------|----------------|----------------|-----------------------|
| 15 | C | C | 60 |
| 16 | C | N | 680 |
| 17 | N | C | 5 |

with respect to the established binding modes for these scaffolds. Subsequently, the FBDD approach was used to try to optimize the active molecules.

(i) Benzothiazoles. Among the benzothiazoles, 2-mercapto-benzothiazole (**1**) displays an IC₅₀ of 50 μM, which is better than the activity of PIM (IC₅₀ of 125 μM under our assay conditions). We subsequently tested some closely related molecules to gain further insight into the structure–activity relationship (Table 1). Interestingly, only the 5-Cl substitution (**2**), placed in pocket A (Figure 4A), was found to be tolerated and to keep the IC₅₀ unchanged. A 6-amino substitution of the benzyl ring abolished activity (**3**). Nitrogen, oxygen, and carbon analogues (**4**–**8**) as well as N-methylated compound **9** showed no activity (Table 1). Inactivity of S-methylated compound **10** might at first sight suggest that the active form requires the free double-bonded sulfur atom. However, our fragment-based virtual lead optimization procedure suggested the addition of a trimethylamino group to the thiol (**11**). This compound recovered the initial activity of **1** and disproves the hypothesis.

In EADock, the three active compounds show a conserved binding mode, with the benzothiazole sulfur pointing toward the heme iron but with the distance being rather large [3.3 Å (Figure 4A,B)]. DFT calculations revealed that the benzothiazole sulfur of compound **1** can bind weakly (binding energy of −2.9 kcal/mol) to the heme iron at a distance of 2.4 Å. In contrast, the benzothiazole nitrogen of compound **1**, which would be expected to bind much stronger in analogy to the binding energy of nitrogen in thiazole (−19.2 kcal/mol), cannot approach the iron sufficiently due to steric hindrance among heme, the benzyl ring, and the thiol sulfur and therefore displays no favorable binding energy (Figure S1 of the Supporting Information). Although EADock is not able to distinguish between active and inactive compounds on the basis of its scoring function, inactive compounds mostly exhibit different binding modes. The loss of inhibitory function upon modification of one atom of the NH–C(=S)–S motif is reminiscent of the same phenomenon with the dithiocarbamate ligands.³¹

(ii) Phenylthiazoles. Another interesting new family of IDO inhibitors consists of the phenylthiazoles (Table 2), with the best IC₅₀ being similar to that of the benzothiazoles (50 μM). The docked structures orient the thiazole sulfur atom toward the heme iron (Figure 4C,D). Also here, replacement of the thiol group (**12**) with an amino group (**13**) strongly decreased activity. Modification of the thiol side chain, as in **11**, also led to a drastically diminished

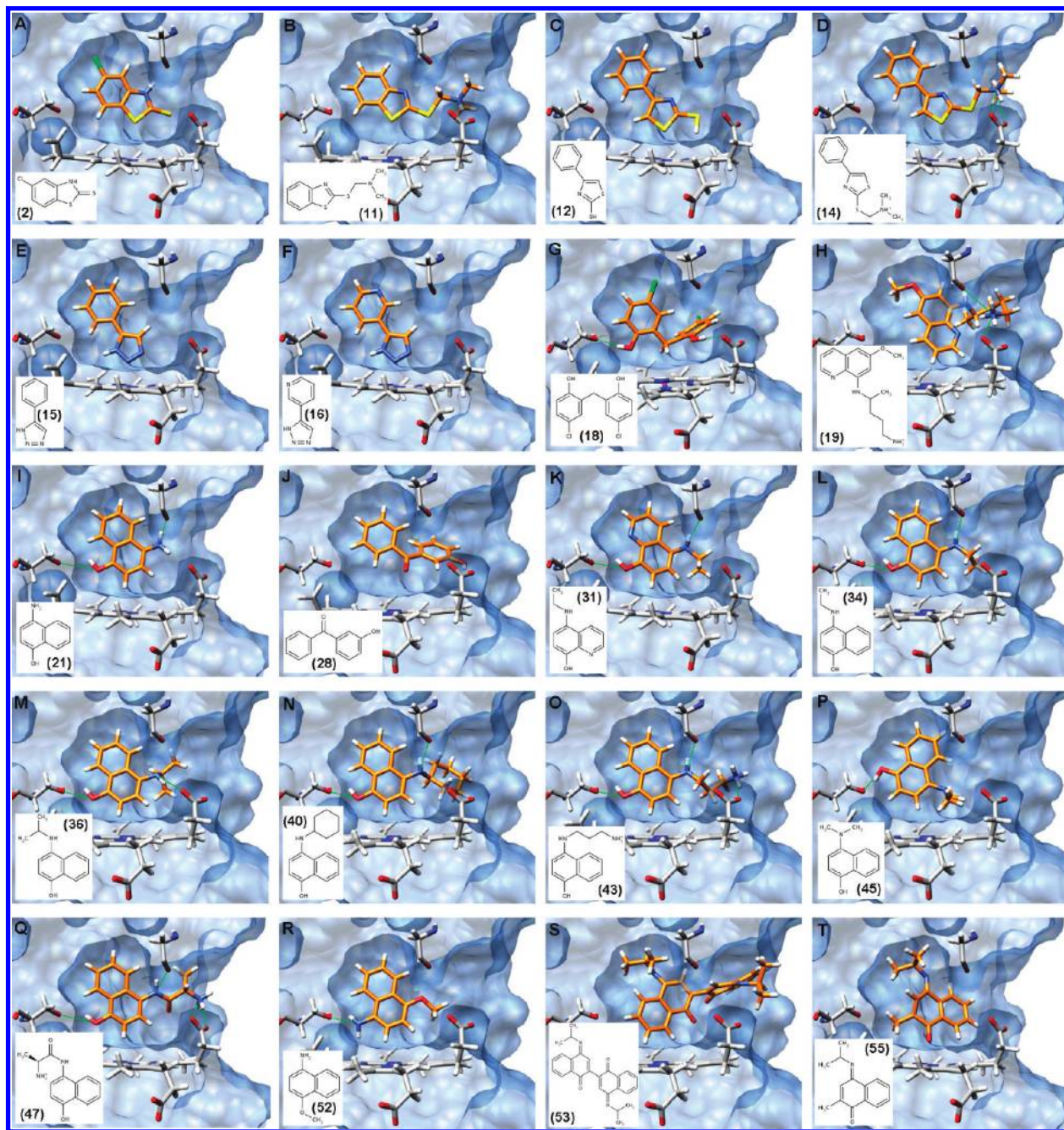


Figure 4. Docked structures of active compounds inside the IDO active site (ligand carbon atoms colored orange, hydrogen bonds colored green, and IDO surface colored blue): (A and B) benzothiazoles, (C and D) phenylthiazoles, (E and F) triazoles, (G and H) FDA-approved compounds, (I and J) hits from FBDD, (K–R) reduced para-substituted quinolines/naphthalenes, and (S and T) oxidized para-substituted quinolines/naphthalenes (compound **53** was docked with AutoDock ⁴⁹ as EADock did not yield a conformation inside the active site).

activity, even though in the docked structure the positively charged amino group is able to form a salt bridge with the heme propionate (Figure 4D).

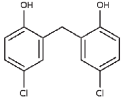
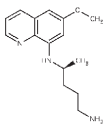
(iii) Triazoles. The triazoles tested (Table 3) are structurally similar to PIM, with the imidazole ring being replaced by a triazole ring. The docked structures also closely resemble PIM, with a nitrogen coordinated to the heme iron (Figure 4E,F). The *m*-pyridyl compound (**16**) is much less active than the phenyl compound (**15**), while the *p*-pyridyl compound (**17**) is 12 times more active than compound **15**. DFT calculations gave binding energies on the order of the experimentally observed activities (−20.39 kcal/mol for **15**, −19.71 kcal/mol for **16**, and −20.72 kcal/mol for **17**). The

binding energies are correlated with the charge of the iron-bound triazole ring in the heme complex (+0.02 for **15**, +0.08 for **16**, and −0.04 for **17**); i.e., the more electronic density is located on the triazole ring, the higher the binding energy and the higher the experimentally observed activity. The low activity of compound **16** is in agreement with the low activity of 4-*m*-pyridylimidazole compared to that of 4-phenylimidazole (PIM) observed previously.³⁵

Screening of FDA-Approved Compounds. We used the developed pharmacophore model as well as results from the fragment-based screening (see below) to guide docking of the collection of FDA-approved compounds provided by the DSSTox⁴⁷ database. A subset of 65 compounds (Figure S2

of the Supporting Information) was chosen for docking on the basis of their scaffolds, which were required to be identical or closely related to one of the active scaffolds found during previous screening. On the basis of the commercial availability and successful docking, five compounds were bought and tested in the enzymatic assay (amodiaquine, primaquine, propranolol, dichlorophene, and oxolamine). This led to the discovery of two compounds with IDO inhibitory activity (Figure 4G,H). The disinfectant, preservative, and biocide dichlorophene (**18**) exhibited an IC_{50} of 70 μ M (Table 4). In addition, the anti-malaria medication primaquine (**19**) displayed an IC_{50} of 50 μ M. Primaquine contains a quinoline, a bioisostere of the indole ring of Trp.

Table 4. Enzymatic Activity of FDA-Approved Compounds

| | Structure | IC_{50} [μ M] |
|-----------|---|----------------------|
| 18 |  | 70 |
| 19 |  | 50 |

Indeed, primaquine might have a potential in cancer treatment, as it has already been approved for use in humans.

Fragment-Based Drug Design. A proof of concept of our fragment-based docking—linking procedure is the emergence of the known IDO inhibitor PIM from the linking of benzene with imidazole (Figure 5). Pose 2 of the benzene map and pose 4 of the imidazole map were identified as being in a good orientation for creation of a link between them. Linking and subsequent docking were in excellent agreement with the crystal structure (rmsd of 0.3 Å).

In our initial FBDD effort, 15 commercially available compounds were identified as promising candidate inhibitors and were tested in the enzymatic assay. Isolated frameworks were also considered for in vitro testing. Eight low-molecular weight inhibitors were identified in this way (Table 5): 5-amino-8-hydroxyquinoline (**20**), 4-amino-1-naphthol (**21**), 4-hydroxycarbazole (**22**), *N*-phenyl-*p*-phenylenediamine (**23**), benzophenone (**24**), 9-fluorenone (**25**), 9-hydroxyfluorene (**26**), and 2-phenoxyaniline (**27**). The success rate of more than 50% highlights the efficiency of the fragment-based virtual lead design approach. Most compounds were found to be only weakly or moderately active, but they all represent straightforward organic frameworks of low molecular weight with many purchasable or easily synthesizable derivatives. A common motif of these molecules is the presence of at least two aromatic rings, optionally joined by a flexible or cyclic linker of one or two atom lengths. However, a few similar compounds have been

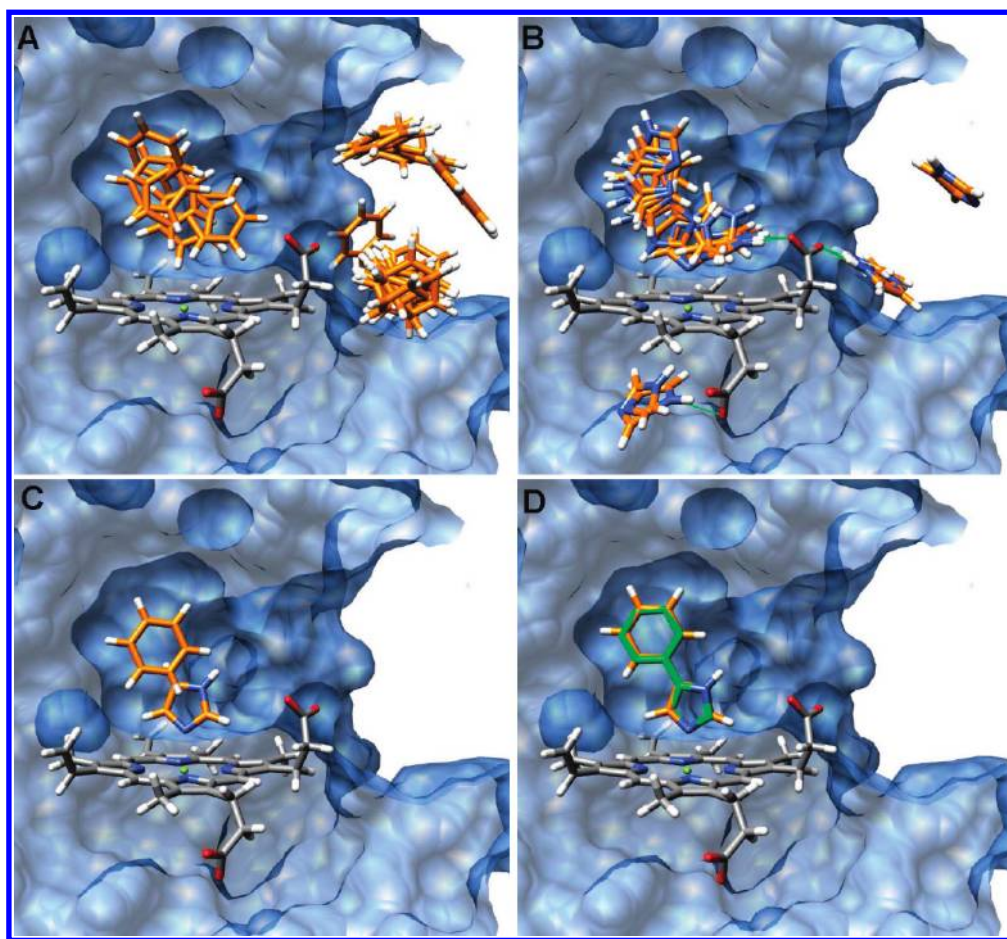
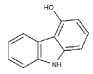
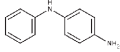
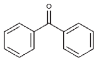
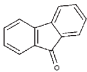
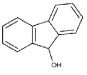
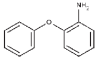
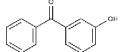
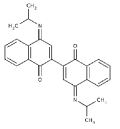
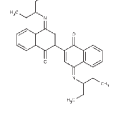
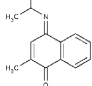


Figure 5. Fragment-based drug design, the test case being 4-phenylimidazole (PIM): (A) map of favorable positions for benzene, (B) map of favorable positions for imidazole, (C) linking of benzene and imidazole due to satisfaction of geometric criteria, and (D) superposition of the best pose from docking of PIM with the X-ray structure.

Table 5. Enzymatic Activity of Diverse Compounds from FBDD

| | Structure | IC ₅₀ [μ M] |
|----|---|-----------------------------|
| 22 |  | 400 |
| 23 |  | 400 |
| 24 |  | 1000 |
| 25 |  | >200 |
| 26 |  | >1000 |
| 27 |  | >1000 |
| 28 |  | 500 |
| 53 |  | 0.45 |
| 54 |  | 0.52 |
| 55 |  | 0.20 |

found not to be active in IDO. The distinction between active and inactive compounds may be due to the low solubility of some compounds, which complicated their testing at the high concentrations required to detect their activity. Benzophenone as well as the most active compounds, the para-substituted quinoline or naphthalene, was chosen for further optimization.

(i) Benzophenones. Benzophenone (**24**) shows IDO inhibitory activity with an IC₅₀ of 1 mM. Our fragment-based lead optimization procedure proposed a hydroxy substitution in the meta position (Figure 4J). This molecule (**28**), which is commercially available, showed an activity higher by a factor of 2 (IC₅₀ = 500 μ M).

(ii) Para-Substituted Quinolines and Naphthalenes. Starting from the frameworks quinoline and naphthalene, bioisosteres of the indole ring of Trp, our optimization procedure proposed 5-amino-8-hydroxyquinoline (**20**) as an IDO inhibitor (Figure 6). This compound, as well as most of the

subsequently tested derivatives, was found to be a potent IDO inhibitor with a high ligand efficiency (Table 6). In most compounds, the OH group and the NH₂ group form hydrogen bonds with Ser167, Gly262, or the heme propionate (Figure 4I–R), but other binding modes are also possible and present among the docking solutions.

The monosubstituted quinoline **30** exhibited very low activity, which underlines the importance of the para substitution of the quinoline and/or naphthalene rings. Compound **45**, which is doubly substituted on the amine group, is 2 orders of magnitude less active than singly substituted **33**. This loss of activity could be due to steric hindrance by the methyl group or due to the loss of a hydrogen bond with the receptor (Figure 4P). When the amino group is used to form an amide bond with an amino acid (Figure 4Q), activity also decreases by 1–2 orders of magnitude (**46–50**).

Comparison of similarly substituted quinolines and naphthalenes (**20** and **21**, **31** and **34**, and **32** and **36**) showed agreement of the measured activities within a factor of 2.5.

We tried to target pocket B in the IDO active site with aliphatic groups [**33–40** (Figure 4L–N)]. Addition of a methyl or an ethyl group as well as the larger isobutyl and cyclohexyl groups decreased activity with respect to unsubstituted compound **21**, but addition of medium-sized aliphatic groups recovered the initial activity of an IC₅₀ of 3–5 μ M. Addition of a positively charged amino group (**43** and **44**) that could form a salt bridge with the heme propionate (Figure 4O), as well as addition of a phenyl ring (**41**), led to the same maximal activity of 3–5 μ M.

Most of the tested quinoline and naphthalene derivatives are redox-active compounds, which were synthesized in the reduced form. Since the incubation medium for the enzymatic assay contained reducing agents (ascorbate and methylene blue), the active reagent is likely to be the reduced form. However, the possibility that their ability to inhibit IDO relies partially or fully on oxidation of the heme iron of IDO cannot be excluded. Similar considerations hold true for the tryptamine quinones and naphthoquinones described previously.^{27,28,33,34} DFT calculations of the binding energies of the oxidized and of the reduced forms of 4-amino-1-naphthol (**21**) show that the reduced form is unlikely to bind directly to the heme iron in IDO, while the oxidized form could bind either through its nitrogen atom (binding energy of –26.8 kcal/mol), when unsubstituted, or through its oxygen atom (–13.8 kcal/mol). Substitution of the nitrogen atom precludes iron coordination due to steric hindrance.

The substituted hydronaphthoquinone **51** displayed an IC₅₀ of 12.5 μ M, while the methoxy-substituted amine **52** (Figure 4R) showed an even higher activity (5.5 μ M). In both compounds, oxidation is hindered by the substituents, therefore arguing against a purely redox-based inhibition mechanism. We tried to synthesize pure oxidized forms of compounds **36** and **39**. However, during synthesis, the compounds dimerized to yield **53** and **54** (Table 5). Activities of these oxidized dimers (Figure 4S) were found to be in the nanomolar range (Table 5), an activity ~10 times higher than that of the reduced forms. To prevent dimerization, methyl-protected compound **55** was synthesized and tested in the enzymatic assay. This compound (Figure 4T) could bind to the heme iron via its oxygen atom and showed an even better IC₅₀ of 200 nM.

Cellular Assays. We tested compounds with a lower IC₅₀ in the enzymatic assay (**1**, **12**, **15**, **17–21**, **29**, **31**, **32**, **34–37**,

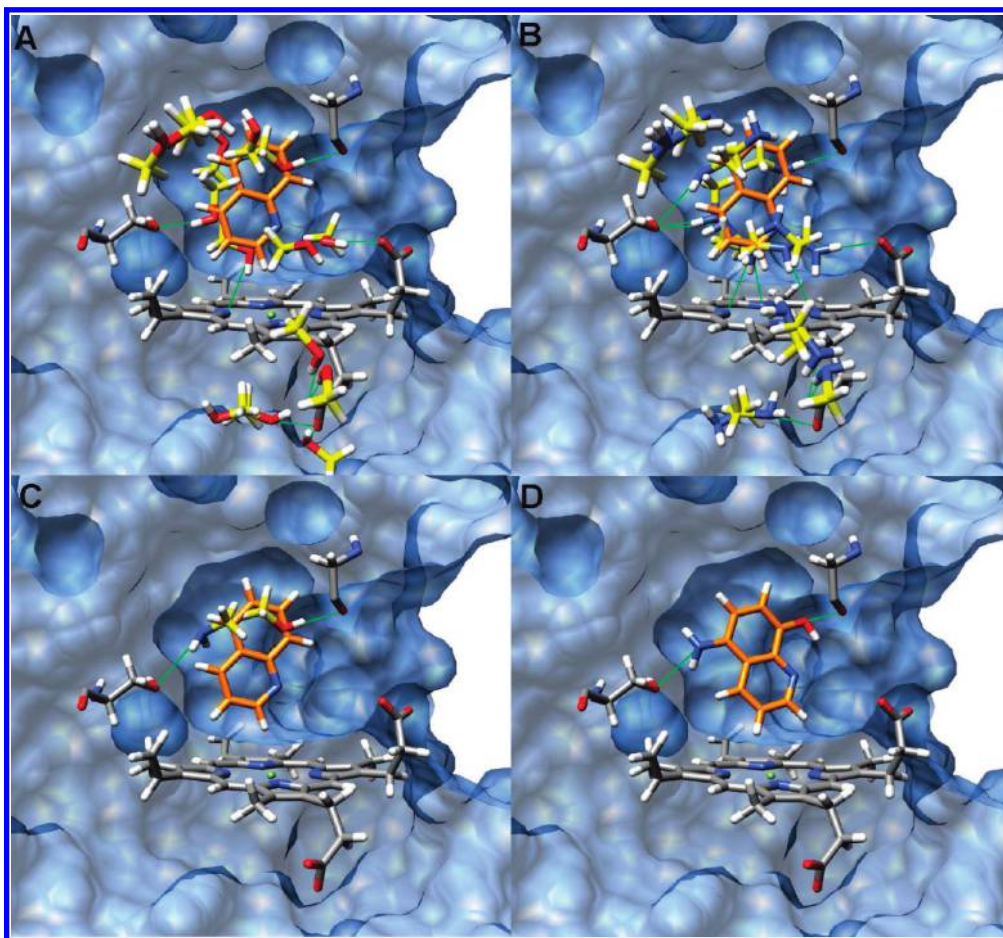


Figure 6. Fragment-based drug design, in the case of 5-amino-8-hydroxyquinoline (**20**): (A) quinoline with a map of favorable positions for methanol, (B) quinoline with a map of favorable positions for methylamine, (C) linking of quinoline with methanol and methylamine due to satisfaction of geometric criteria, and (D) docked pose of compound **20**.

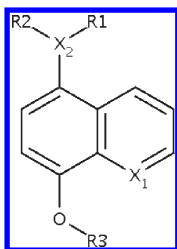
and **53–55**) for their ability to inhibit tryptophan degradation and kynurenine production in cells expressing either murine or human IDO. Active compounds were also screened for their inhibitory activity in cells expressing murine TDO to investigate their selectivity. For all cell lines, cell viability was evaluated at the end of the assay. This cellular assay is informative for drug development as it evaluates not only the IDO/TDO inhibitory effect of the compounds but also their capacity to permeate the cell, their potential cytotoxicity, inhibition of tryptophan transporters, and the effects of their metabolites. We first used cells expressing mouse IDO and tested compounds at a concentration of 2, 20, or 200 μM . A series of compounds was less active for IDO inhibition than our reference molecule, L-1MT ($\text{IC}_{50} = 40 \mu\text{M}$ on murine IDO), and not further characterized. This was the case for triazole compound **17**, FDA-approved compounds **18** and **19**, and quinoline and/or naphthalene compounds **21**, **31**, **32**, **35**, and **37** (Table 7). For the other compounds, we then determined IC_{50} and LD_{50} values in more detailed dose–response curves using mouse and human IDO-expressing cells. Dose–response curves for the inhibition of tryptophan degradation and the inhibition of kynurenine production were superimposable in most cases (Figure 7A). For IC_{50} calculation, we used the values of tryptophan degradation, and we considered only those concentrations of a compound permitting at least 75% of cell viability (Figure 7A). For quinoline **20**, we observed an IC_{50} of 1.0 μM in cells expressing mouse IDO. However, because

this compound is toxic at a low concentration (5 μM), we did not determine its IC_{50} in cells expressing human IDO (Table 7).

Interestingly, substituted naphthalenes **34** and **36** exhibited good activity in the cellular assay against hIDO, while the corresponding quinolines **31** and **32** were inactive. This finding is at variance with the enzymatic assay, where quinolines and naphthalenes showed a comparable activity. In general, the correlation between the measured IC_{50} in the enzymatic and in the cellular assay is low, emphasizing the importance of cellular tests early in the drug design process.

For most compounds (**1**, **12**, **29**, **34**, **36**, **53**, and **54**), the IC_{50} values obtained with human IDO were similar or better than those obtained with mouse IDO (Table 7 and Figure 7B). However, for compounds **15** and **55**, the IC_{50} obtained with human IDO was ~ 10 -fold higher than the one obtained with mouse IDO (Table 7). Such a difference might result either from a genuine difference in the inhibition of mouse and human IDO or from differences between mouse and human cells in the other aspects assessed by the cellular assay, including effects on the transporters or the effect of metabolites.

The best inhibitors of hIDO in the cellular assay are phenylthiazole **12** and benzothiazole **1** [IC_{50} values of 4.0 and 7.0 μM (Table 7 and Figure 7B)], which displayed 7–12 times higher activities than in the enzymatic assay. All other active compounds exhibited either comparable activities in cellular and enzymatic assays with hIDO (**15**, **20**, **29**, **34**, and **36**),

Table 6. Enzymatic Activity of Para-Substituted Quinolines and Naphthalenes

| | X ₁ | X ₂ | R ₁ | R ₂ | R ₃ | IC ₅₀ (μM) |
|----|----------------|----------------|--|-----------------|-----------------|-----------------------|
| 20 | N | N | H | H | H | 3 |
| 21 | C | N | H | H | H | 6 |
| 29 | C | O | H | — | H | 1.5 |
| 30 | N | H | — | — | H | 750 |
| 31 | N | N | CH ₂ CH ₃ | H | H | 40 |
| 32 | N | N | CH(CH ₃) ₂ | H | H | 15 |
| 33 | C | N | CH ₃ | H | H | 12.5 |
| 34 | C | N | CH ₂ CH ₃ | H | H | 16 |
| 35 | C | N | CH ₂ CH ₂ CH ₃ | H | H | 4.5 |
| 36 | C | N | CH(CH ₃) ₂ | H | H | 2.5 |
| 37 | C | N | C(CH ₃) ₃ | H | H | 4 |
| 38 | C | N | CH ₂ CH(CH ₃) ₂ | H | H | 25 |
| 39 | C | N | (CH)(CH ₂ CH ₃) ₂ | H | H | 3.5 |
| 40 | C | N | cyclohexyl | H | H | 15 |
| 41 | C | N | CH ₂ -phenyl | H | H | 2.5 |
| 42 | C | N | (CH ₂) ₂ NH ₂ | H | H | 44 |
| 43 | C | N | (CH ₂) ₃ NH ₂ | H | H | 5 |
| 44 | C | N | (CH ₂) ₂ N(C ₂ H ₅) ₂ | H | H | 3 |
| 45 | C | N | CH ₃ | CH ₃ | H | 1000 |
| 46 | C | N | glycyl | H | H | 105 |
| 47 | C | N | L-alanyl | H | H | 60 |
| 48 | C | N | D-alanyl | H | H | 90 |
| 49 | C | N | L-seryl | H | H | 400 |
| 50 | C | N | L-prolyl | H | H | 200 |
| 51 | C | O | CH ₂ CH ₂ OH | — | H | 12.5 |
| 52 | C | N | H | H | CH ₃ | 5.5 |

or they exhibited a significantly reduced activity in the cellular assay (**53–55**).

For a large number of compounds, their IC₅₀ value for mouse TDO could not be determined because of low cell viability. In general, however, naphthalene-derived compounds **29**, **34**, **36**, and **53–55** did not seem to display a good selectivity for hIDO over mTDO, while compounds **1**, **12**, and **15** showed no significant inhibitory effect against mTDO up to the highest concentrations, which demonstrates their good selectivity for IDO over TDO.

The “therapeutic index” of compounds **1**, **12**, **15**, **29**, **34**, **36**, and **54** was found to be good, with LD₅₀ values 5–20 times higher than the respective IC₅₀ values. However, for compounds **53** and **55**, the IC₅₀ and LD₅₀ values are very similar, which might hinder their in vivo testing.

In summary, 10 of the newly discovered IDO inhibitors showed significant IDO inhibition also in the cellular assay. Seven of these compounds demonstrated a low cytotoxicity (**1**, **12**, **15**, **29**, **34**, **36**, and **54**), and three of these compounds additionally showed a good selectivity for IDO versus TDO (**1**, **12**, and **15**).

Summary

In this work, we have used two strategies for the rational design of new potent IDO inhibitors, which have shown promising results.

By pharmacophore-based lead design, we discovered three families with IDO inhibitory activity: benzothiazoles, phenylthiazoles, and triazoles. One compound of each respective family (**1**, **12**, and **15**) also showed good results in the cellular assays with low cytotoxicities, higher activities against IDO than the reference compound L-1MT, and a good selectivity with respect to TDO. Additionally, we identified two FDA-approved compounds, dichlorophene (**18**) and primaquine (**19**), which showed a measurable activity in the enzymatic assay. Here, especially the anti-malaria primaquine is of great interest as it has already been approved for use in humans.

Table 7. Cellular Assay for IDO and TDO Inhibition^a

| | IC ₅₀ (μM) | | | LD ₅₀ (μM) | | | enzymatic IC ₅₀ (μM) |
|-------|-----------------------|------|-------|-----------------------|---------|--------|---------------------------------|
| | mIDO | hIDO | mTDO | mIDO | hIDO | mTDO | hIDO |
| L-1MT | 40 | 90 | > 400 | > 1000 | > 400 | > 400 | ND |
| 17 | NI | ND | ND | 200 | ND | ND | 5.0 |
| 18 | NI | ND | ND | 0.2–2 | ND | ND | 70 |
| 19 | NI | ND | ND | 200 | ND | ND | 50 |
| 21 | NI | ND | ND | 2–20 | ND | ND | 6.0 |
| 31 | NI | ND | ND | 20–200 | ND | ND | 40 |
| 32 | NI | ND | ND | > 200 | ND | ND | 15 |
| 35 | NI | ND | ND | 20–200 | ND | ND | 4.5 |
| 37 | NI | ND | ND | 20–200 | ND | ND | 4.0 |
| <hr/> | | | | | | | |
| 1 | 20 | 7.0 | > 80 | > 80 | > 80 | > 80 | 50 |
| 12 | 20 | 4.0 | > 80 | > 80 | > 80 | > 80 | 50 |
| 15 | 5.0 | 70 | > 400 | > 80 | > 400 | > 400 | 60 |
| 20 | 1.0 | ND | 5.0 | 2.5–5 | ND | 5–10 | 3.0 |
| 29 | 10 | 10 | > 10 | 40–80 | 40–80 | 10–20 | 1.5 |
| 34 | 50 | 50 | > 50 | 400 | 200–00 | 50–100 | 16 |
| 36 | 30 | 12.5 | > 15 | > 80 | 100–200 | 15–20 | 2.5 |
| 53 | > 50 | 25 | > 50 | 50 | 50 | 100 | 0.45 |
| 54 | > 200 | 50 | > 50 | 200 | > 400 | 100 | 0.52 |
| 55 | 4.0 | > 50 | 6.3 | 15–20 | 50 | 10 | 0.20 |

^a IC₅₀ and LD₅₀ values of different compounds tested in cells transfected with mouse IDO (mIDO), human IDO (hIDO), or mouse TDO (mTDO). NI, no significant IDO inhibition by comparison to L-1MT. ND, not determined. For comparison, also the IC₅₀ measured in the enzymatic assay is given.

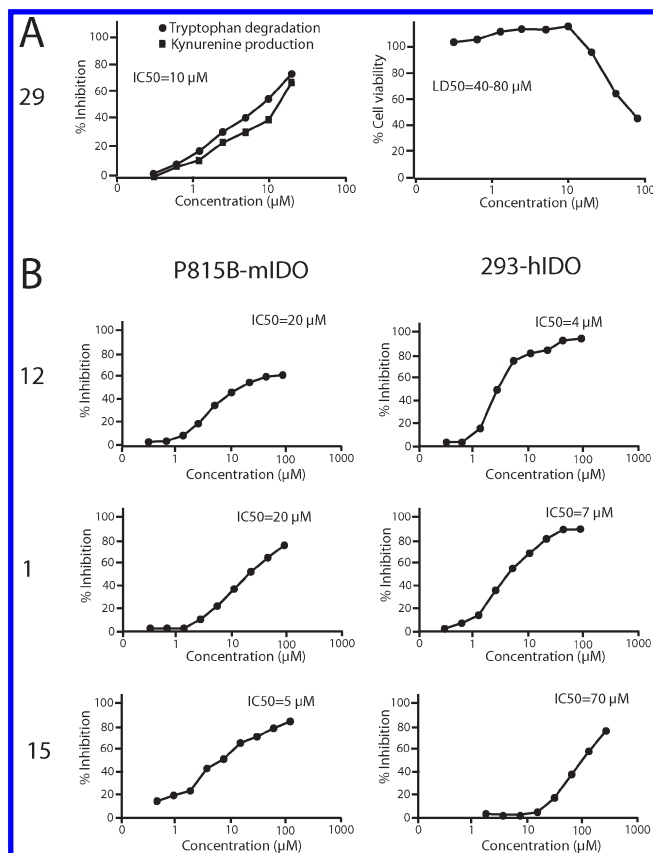


Figure 7. Dose response for IDO inhibition in a cellular assay. (A) IDO inhibition and cytotoxicity of compound **29** tested on 293-hIDO cells. The left graph shows the percent of IDO inhibition. The right graph shows the cell viability, measured in an MTT assay. The two higher concentrations of the viability curve (right) were excluded from the IDO inhibition curve (left) as the viability was below 75%. (B) Dose response for IDO inhibition in a murine (left) or human (right) cellular assay. The graph shows the percent of IDO inhibition tested on P815B-mIDO cells (left) and on 293-hIDO cells (right) related to the concentration of compounds **12**, **1**, and **15**.

However, cellular assays showed a cytotoxicity higher than its activity.

By fragment-based virtual lead design, we obtained eight completely new scaffolds with IDO inhibitory activity from a total of 15 compounds that were tested in the enzymatic assay. Most of these compounds are only weak or moderate IDO inhibitors, with the exception of the para-substituted quinolines and naphthalenes that have an activity in the low micromolar range. At the time of discovery, this framework did not resemble any known IDO inhibitor. A large ensemble of substitutions of 4-amino-1-naphthol can be undertaken without significantly altering the IC₅₀ of ~1–10 μM. However, disubstitution or deletion of the amine group, as well as to a lesser extent its amidation, led to a significantly reduced activity. In cellular assays, two of the 4-alkylamino-1-naphthol compounds (**34** and **36**) exhibited good activity against IDO and low cytotoxicity. As most of these compounds exist in two oxidation states, we also tested three oxidized compounds (**53–55**). In the enzymatic assay, these compounds showed an IC₅₀ of 200–500 nM and are thus the most active IDO inhibitors described in this work. In cellular assays, however, these compounds showed slightly worse results than reduced compounds **34** and **36**.

In summary, we have used our docking algorithm EADock, in combination with a fragment-based drug discovery strategy,

to successfully design new IDO inhibitors with good ligand efficiency in vitro. Some compounds show promising results in the cellular assay and will be evaluated in vivo in the future. Not all discovered scaffolds have yet been investigated in detail. Lead optimization of some of the weakly active hits may potentially yield additional potent IDO inhibitors.

Experimental Section

Docking. The docking algorithm EADock^{45,46} combines the sampling power of a multiobjective hybrid evolutionary algorithm with the physical scoring function of the CHARMM22 force field.^{74,75} In brief, a population of ligand binding modes is modified by various stochastic and semistochastic operators and evaluated using two scoring functions. Individual binding modes are evaluated by the fast and efficient SimpleFitness, which is used to drive the search. Simultaneously, clusters of binding modes are evaluated by the more selective yet slower FullFitness, which accounts for the solvation free energy using the analytical GB-MV2 model.⁷⁶ Binding modes with a favorable SimpleFitness but an unfavorable FullFitness are removed from the accessible search space using a blacklisting procedure. This dynamic adjustment of the search space according to the evolutionary path prevents the refinement of suboptimal binding modes. Several improvements for blind docking applications have been implemented recently in EADock.⁴⁶

Dockings were performed using the parameters described in ref 45. In brief, 250 initial binding modes were generated by random translation and rotation of the ligand followed by a sequential optimization of each rotatable dihedral angle. In each generation of the evolutionary algorithm, 10% of the population was renewed, and a total of 400 generations were computed. The maximum allowed distance between the center of the binding site and explored binding modes was 15 Å. The protein was kept fixed during the docking.

A Morse-like metal binding potential (MMBP) is used to describe the interactions between the heme iron of IDO and ligand atoms that display a free electron pair for iron binding.⁷³

A successful docking was reported when at least one of the 10 top-ranked clusters (i) entered into pocket A of the active site (minimal distance between the ligand and the sulfur atom of Cys129 of < 5.2 Å) and (ii) adopted a binding mode resembling the most favorable binding mode of related ligands with a similar or identical scaffold if existent (visual inspection).

We use the PIM-bound X-ray structure (PDB entry 2D0T, chain A) as a scaffold, because it has a higher resolution and provides a larger binding site than the cyanide-bound structure (PDB entry 2D0U).¹⁴ In addition to PIM, there are two molecules of 2-(*N*-cyclohexylamino)ethanesulfonic acid bound at the entrance of the binding site. Since they are likely to interfere with the binding modes of ligands other than PIM, they were removed during setup.

Fragment Docking and Linking. A library of 26 frameworks and 29 side chains (Figures 7.2 and 7.3 in ref 77; see also Figures S3 and S4 of the Supporting Information) was extracted from common features of commercially available drugs.^{54,55} These have been docked independently to determine maps of favorable binding modes. In each generation of the evolutionary algorithm, 10% of the population of 500 binding modes was renewed. For clustering, a cutoff of 1.2 Å was used and the maximum cluster size was chosen to be 5. The blacklisting procedure was switched off to allow exploration of all favorable clusters, not only the best one. All other parameters were the same as in a molecular docking described above. The best poses of the 50 best clusters were considered for linking if they displayed an rmsd of less than 10 Å from the starting position inside the active site. A link between a framework and a side chain was proposed if the distances and angles between connecting atoms were in agreement with standard bond distances and angles depending on their hybridization. For aromatic frameworks,

the planarity of the aromatic atom was enforced. In a second step, a check for steric clashes between newly connected fragments was conducted.

Virtual lead design has been performed by linking all side chains with all frameworks. Small frameworks (six or fewer heavy atoms) were alternatively considered as side chains and linked with other frameworks. Linking was also applied for lead optimization purposes by linking side chains to active compounds.

Density Functional Theory Calculations. Quantum chemical geometry optimizations were conducted in the density functional theory (DFT) framework using the Quickstep code,^{78,79} which is part of the CP2K program package.⁸⁰ We used Goedecker–Teter–Hutter (GTH) pseudopotentials,^{81,82} the Perdew–Burke–Ernzerhof functional,⁸³ a density cutoff of 280 Ry, and the TZV2P basis set except for iron (QZV basis set).⁷⁹ All calculations were conducted in an isolated cubic cell with an edge length of 20 Å, using the multipole decoupling scheme of periodic images. Geometry optimizations were conducted with the L-BFGS method⁸⁴ using the standard convergence criteria. Atomic point charges were calculated from plane-wave-expanded densities using a fit to atom-centered Gaussians.⁸⁵

The histidine-bound heme complex of IDO was modeled with an iron–porphyrin–imidazole system. Binding energies were calculated by subtracting the energy of the iron–porphyrin–imidazole system and the energy of the isolated ligand from the energy of the 6-fold coordinated system. For the ferrous iron–porphyrin–imidazole system, the ground state with DFT gradient-corrected functionals is a triplet.⁸⁶ For the 6-fold coordinated systems, a low-spin complex was always assumed, as it has been found before for closed-shell ligands.⁸⁶ For the case of one distal ligand (imidazole), we checked that the basis set superposition error (BSSE) does not amount to more than 1 kcal/mol with the employed basis sets.

Chemistry. (i) **General Remarks.** Reagents were purchased from Acros, Fluka, Senn, Sigma-Aldrich, or Merck and used without further purification. For extraction and chromatography, all solvents were distilled prior to use. Anhydrous THF, diethyl ether, and toluene were distilled from sodium and benzophenone; dichloromethane was distilled from CaH₂ and methanol from magnesium. Reactions were monitored by thin layer chromatography (TLC) using silica gel plates (Merck 60 F254). Developed TLC plates were visualized with UV light (254 nm) or molybdc reagent [21 g of (NH₄)₆Mo₇O₂₄·4H₂O, 1 g of Ce(SO₄)₂, 31 mL of H₂SO₄, and 470 mL of H₂O]. Flash chromatography (FC) was conducted using silica gel 60 Å, 230–400 mesh (Merck 9385). Melting points were measured with a Mettler FP52 apparatus and are uncorrected. Optical rotations were measured with a JASCO DIP-370 digital polarimeter. UV spectra were recorded on a Kontron Uvikon 810 CW spectrophotometer. IR spectra were recorded on a Perkin-Elmer Paragon 1000 FT-IR spectrometer. Mass spectra were recorded on a Nermag R 10-10C instrument in chemical ionization mode. Electrospray mass analyses were recorded on a Finnigan MAT SSQ 710C spectrometer in positive ionization mode. ¹H NMR spectra were recorded on a Bruker DPX-400 FT, Bruker ARX-400 FT, or Bruker AMX-600 spectrometer. All ¹H signal assignments were confirmed by COSY spectra. ¹³C NMR spectra were recorded on a Bruker DPX-400 FT (100.61 MHz) or on a Bruker ARX-400 FT (100.61 MHz) spectrometer. All ¹³C signal assignments were confirmed by HMQC spectra. Chemical shifts are given in parts per million, relative to an internal standard such as residual solvent signals. Coupling constants are given in hertz. High-resolution mass spectra were recorded via ESI-TOF-HRMS or MALDI-TOF-HRMS. The purity of all novel compounds was confirmed to exceed 95% by NMR and high-resolution mass spectra.

(ii) **General Procedures.** (a) **General Procedure for Reductive Amination.** 4-Amino-1-naphthol hydrochloride or 5-amino-8-hydroxyquinoline dihydrochloride and the carbonyl compound

were suspended in 1,2-dichloroethane and treated with 2 equiv of acetic acid; 1.7 equiv of NaBH(OAc)₃ was added in portions, and the mixture was stirred at ambient temperature for 12 h. An aqueous NaHCO₃ solution was added at 0 °C until a basic pH was obtained. The aqueous phase was extracted with diethyl ether (4 × 50 mL). The combined organic phases were dried and concentrated in vacuo to afford the crude product which was purified by FC (4:1 light petroleum ether/diethyl ether mixture) to give compounds **31**, **32**, **34–36**, **39**, and **40** in 81, 96, 70, 82, 94, 92, and 88% yield, respectively. The corresponding hydrochloric salt was obtained by treating the amine in diethyl ether with dry hydrochloric acid in 2-propanol or dioxane. The precipitate was filtered, washed with diethyl ether, and recrystallized from ethyl acetate and methanol.

(b) **General Procedure for Nucleophilic Addition.** *p*-Naphtho-hydroquinone was dissolved in toluene before addition of 1.1 equiv of amine and the mixture was refluxed for 1 h. The solution was concentrated in vacuo, and the crude product was purified by FC (4:1 light petroleum ether/diethyl ether mixture). The procedure gave naphthalenes **38** and **41–44** in 89, 65, 95, 77, and 84% yield, respectively. The corresponding hydrochloric salt was obtained as described in the reductive amination procedure. For the Boc-protected terminal amine compounds, deprotection and formation of the dihydrochloric salts were conducted by treatment with HCl and methanol in dry diethyl ether.

(c) **General Procedure for Amino Acid Coupling.** To a solution of a Boc-protected amino acid (1.05 equiv) suspended in CH₂Cl₂ was added TBS-protected 4-amino-1-naphthol hydrochloride (1.0 equiv) at 0 °C. After the mixture had been stirred for 15 min, a mixture of 1-hydroxy-7-aza-1,2,3-benzotriazole (HOAt, 1.5 equiv), *O*-(7-azabenzotriazol-1-yl)-1,1,3,3-tetramethyluronium hexafluorophosphate (HATU, 1.5 equiv), and sym-collidine (3 equiv) was added. The reaction mixture was stirred at 0 °C for 1 h, followed by addition of ethyl acetate to stop the reaction. The solution was quenched with 5% aqueous HCl (10 mL), washed successively with a saturated aqueous solution of NaHCO₃ (5 mL), water, and brine, and dried (MgSO₄). Evaporation of the filtrate and FC (1:1 light petroleum ether/ethyl acetate mixture) gave a solid of naphthalenes **46–50** in 90, 94, 93, 85, and 83% yield, respectively. Chromatography was followed by Boc deprotection and preparation of the corresponding hydrochloric salt as outlined above.

(d) **General Procedure for Oxidation with Ag₂O.** To a solution of 1.0 equiv of *p*-aminoalkyl-1-naphthol and 1.2 equiv of Na₂SO₄ in diethyl ether (0.01 M) was added 0.5 equiv of Ag₂O, and the mixture was stirred for 1 h. The filtrate was diluted with 50 mL of water. The aqueous phase was extracted with diethyl ether (2 × 50 mL). The combined organic phases were dried and concentrated in vacuo. FC (9:1 pentane/diethyl ether mixture) gave the pure compounds **53–55** in 45, 56, and 61% yield, respectively.

(e) **5-(Ethylamino)quinolin-8-ol Dihydrochloride (31).** Product **31** was synthesized from 5-amino-8-hydroxyquinoline dihydrochloride and acetaldehyde according to the reductive amination procedure to afford a yellow oil in 81% yield. Mp: 224–225 °C. TLC: *R*_f = 0.38 (30% diethyl ether/pentane). ¹H NMR (400 MHz, DMSO-*d*₆) δ 9.52 (bs, 1H, NH), 8.82 [dd, 1H, ³*J*(H-C(2), H-C(3)) = 4.5, ⁴*J*(H-C(2), H-C(4)) = 1.5, H-C(2)], 8.56 [dd, 1H, ³*J*(H-C(4), H-C(3)) = 8.5, ⁴*J*(H-C(4), H-C(2)) = 1.5, H-C(4)], 7.48 [dd, 1H, ³*J*(H-C(3), H-C(4)) = 8.5, ³*J*(H-C(3), H-C(2)) = 4.5, H-C(3)], 7.14 [d, 1H, ³*J*(H-C(7), H-C(6)) = 8.0, H-C(7)], 7.06 [d, 1H, ³*J*(H-C(6), H-C(7)) = 8.0, H-C(6)], 2.93 [dd, 2H, ²*J* = 14.5, ³*J*(H-C(1'), H-C(2')) = 7.0, H-C(1')], 0.82 [m, 3H, ³*J*(H-C(2'), H-C(1')) = 7.0, H-C(2')]. ¹³C NMR (100.6 MHz, DMSO-*d*₆): δ 150.2 [s, C(8)], 148.2 [d, ¹*J*(C,H) = 178, C(2)], 139.4 [s, C(9)], 138.4 [s, C(5)], 132.8 [d, ¹*J*(C,H) = 159, C(4)], 127.6 [s, C(10)], 121.5 [d, ¹*J*(C,H) = 165, C(3)], 120.5 [d, ¹*J*(C,H) = 157, C(7)], 110.9 [d, ¹*J*(C,H) = 160, C(6)], 48.8 [t, ¹*J*(C,H) = 134, C(1')], 12.7 [q, ¹*J*(C,H) = 125, C(2')].

ESI-TOF-HRMS: m/z calcd for (M) $C_{11}H_{12}N_2O$ 188.0950, found 188.1001.

(f) 5-(Isopropylamino)quinolin-8-ol Dihydrochloride (32). Product **32** was synthesized from 5-amino-8-hydroxyquinoline dihydrochloride and acetone according to the reductive amination procedure to afford a white solid in 96% yield. Mp: 220–222 °C. TLC: R_f = 0.41 (30% diethyl ether/pentane). 1H NMR (400 MHz, DMSO- d_6): δ 8.79 [d, 1H, $^3J(H-C(2), H-C(3))$ = 4.5, H-C(2)], 8.70 (bs, 1H, NH), 8.56 [d, 1H, $^3J(H-C(4), H-C(3))$ = 8.5, H-C(4)], 7.44 [dd, 1H, $^3J(H-C(3), H-C(4))$ = 8.5, $^3J(H-C(3), H-C(2))$ = 4.5, H-C(3)], 6.99 [d, 1H, $^3J(H-C(7), H-C(6))$ = 8.0, H-C(7)], 6.49 [d, 1H, $^3J(H-C(6), H-C(7))$ = 8.0, H-C(6)], 5.32 (bs, 1H, OH), 3.61 [m, 1H, $^3J(H-C(1'), H-C(2'))$ = 6.0, H-C(1')], 1.21 [d, 6H, $^3J(H-C(2'), H-C(1'))$ = 6.0, H-C(2')]. ^{13}C NMR (100.6 MHz, DMSO- d_6): δ 148.1 [d, $^1J(C,H)$ = 178, C(2)], 144.0 [s, C(8)], 139.4 [s, C(9)], 136.5 [s, C(5)], 131.7 [d, $^1J(C,H)$ = 159, C(4)], 119.9 [d, $^1J(C,H)$ = 165, C(3)], 119.8 [s, C(10)], 112.0 [d, $^1J(C,H)$ = 157, C(7)], 106.0 [d, $^1J(C,H)$ = 160, C(6)], 44.3 [d, $^1J(C,H)$ = 139, C(1')], 22.8 [q, $^1J(C,H)$ = 131, C(2')]. ESI-TOF-HRMS: m/z calcd for (M + H) $C_{12}H_{15}N_2O$ 203.1184, found 203.1178.

(g) 4-(Ethylamino)-1-naphthol Hydrochloride (34). Product **34** was synthesized from 4-amino-1-naphthol hydrochloride and acetaldehyde according to the reductive amination procedure to afford a black solid in 70% yield. Mp: 210–212 °C. TLC: R_f = 0.42 (30% diethyl ether/pentane). 1H NMR (400 MHz, DMSO- d_6): δ 9.82 (bs, 1H, NH), 8.22 [d, 1H, $^3J(H-C(8), H-C(7))$ = 8.0, H-C(8)], 8.16 [d, 1H, $^3J(H-C(5), H-C(6))$ = 8.0, H-C(5)], 7.58–7.38 [m, 2H, H-C(6), H-C(7)], 7.07 [d, 1H, $^3J(H-C(2), H-C(3))$ = 8.0, H-C(2)], 6.87 [d, 1H, $^3J(H-C(3), H-C(2))$ = 8.0, H-C(3)], 3.06–2.97 [m, 2H, H-C(1')], 0.95–0.87 [m, 3H, H-C(2')]. ^{13}C NMR (100.6 MHz, DMSO- d_6): δ 150.1 [s, C(1)], 138.9 [s, C(4)], 133.0 [s, C(9)], 125.9 [s, C(10)], 125.9 [d, $^1J(C,H)$ = 158, C(7)], 124.8 [d, $^1J(C,H)$ = 160, C(6)], 123.9 [d, $^1J(C,H)$ = 127, C(8)], 122.6 [d, $^1J(C,H)$ = 128, C(5)], 119.5 [d, $^1J(C,H)$ = 155, C(2)], 108.9 [d, $^1J(C,H)$ = 158, C(3)], 48.7 [t, $^1J(C,H)$ = 137, C(1')], 12.9 [dd, $^1J(C,H)$ = 125, C(2')]. ESI-TOF-HRMS: m/z calcd for (M) $C_{12}H_{13}NO$ 187.0997, found 187.1119.

(h) 4-(Propylamino)-1-naphthol Hydrochloride (35). Product **35** was synthesized from 4-amino-1-naphthol hydrochloride and propionaldehyde according to the reductive amination procedure to afford a black solid in 82% yield. Mp: 213–215 °C. TLC: R_f = 0.44 (30% diethyl ether/pentane). 1H NMR (400 MHz, DMSO- d_6): δ 9.86 (bs, 1H, NH), 8.30 [m, 1H, $^3J(H-C(8), H-C(7))$ = 8.0, H-C(8)], 8.16 [d, 1H, $^3J(H-C(5), H-C(6))$ = 8.0, H-C(5)], 7.48–7.38 [m, 2H, H-C(6), H-C(7)], 7.10 [d, 1H, $^3J(H-C(2), H-C(3))$ = 8.0, H-C(2)], 6.88 [d, 1H, $^3J(H-C(3), H-C(2))$ = 8.0, H-C(3)], 3.50 (bs, 1H, OH), 2.97–2.87 [m, 2H, H-C(1')], 1.41–1.30 [m, 2H, H-C(2')], 0.83–0.75 [m, 3H, H-C(3')]. ^{13}C NMR (100.6 MHz, DMSO- d_6): δ 150.2 [s, C(1)], 136.5 [s, C(4)], 132.8 [s, C(9)], 125.9 [s, C(10)], 125.9 [d, $^1J(C,H)$ = 155, C(7)], 124.8 [d, $^1J(C,H)$ = 162, C(6)], 123.8 [d, $^1J(C,H)$ = 129, C(8)], 122.7 [d, $^1J(C,H)$ = 127, C(5)], 119.8 [d, $^1J(C,H)$ = 153, C(2)], 108.2 [d, $^1J(C,H)$ = 159, C(3)], 57.2 [t, $^1J(C,H)$ = 140, C(1')], 44.5 [t, $^1J(C,H)$ = 135, C(2')], 12.1 [dd, $^1J(C,H)$ = 127, C(3')]. ESI-TOF-HRMS: m/z calcd for (M + H) $C_{13}H_{16}NO$ 202.1232, found 202.1234.

(i) 4-(Isopropylamino)-1-naphthol Hydrochloride (36). Product **36** was synthesized from 4-amino-1-naphthol hydrochloride and acetone according to the reductive amination procedure to afford a black solid in 94% yield. Mp: 220–223 °C. TLC: R_f = 0.46 (30% diethyl ether/pentane). 1H NMR (400 MHz, DMSO- d_6): δ 9.14 (bs, 1H, NH), 8.14 [m, 2H, H-C(5), H-C(8)], 7.45–7.39 [m, 2H, H-C(6), H-C(7)], 6.77 [d, 1H, $^3J(H-C(2), H-C(3))$ = 8.0, H-C(2)], 6.44 [d, 1H, $^3J(H-C(3), H-C(2))$ = 8.0, H-C(3)], 4.95 (bs, 1H, OH), 3.70–3.60 [m, 1H, H-C(1')], 1.27–1.22 [m, 6H, H-C(2')]. ^{13}C NMR (100.6 MHz, DMSO- d_6): δ 144.5 [s, C(1)], 136.5 [s, C(4)], 126.0 [s, C(9)], 125.4 [s, C(10)], 124.8 [d, $^1J(C,H)$ = 158, C(7)], 124.7 [d, $^1J(C,H)$ = 160, C(6)], 122.7 [d, $^1J(C,H)$ = 127, C(8)], 122.4 [d, $^1J(C,H)$ = 128, C(5)], 109.1

[d, $^1J(C,H)$ = 155, C(2)], 105.9 [d, $^1J(C,H)$ = 158, C(3)], 44.5 [t, $^1J(C,H)$ = 137, C(1')], 23.9 [dd, $^1J(C,H)$ = 125, C(2')]. ESI-TOF-HRMS: m/z calcd for (M + H) $C_{13}H_{16}NO$ 202.1232, found 202.1229.

(j) 4-(Isobutylamino)-1-naphthol (38). Product **38** was synthesized from naphthalene-1,4-diol and isobutylamine according to the nucleophilic addition procedure to afford a black oil in 89% yield. TLC: R_f = 0.56 (30% diethyl ether/pentane). 1H NMR (400 MHz, DMSO- d_6): δ 9.12 (bs, 1H, NH), 8.17 [m, 2H, H-C(5), H-C(8)], 7.48 [m, 2H, H-C(6), H-C(7)], 6.81 [d, 1H, $^3J(H-C(2), H-C(3))$ = 8.0, H-C(2)], 6.42 [d, 1H, $^3J(H-C(3), H-C(2))$ = 8.0, H-C(3)], 5.34 (bs, 1H, OH), 2.99 [m, 2H, H-C(1'), H-C(2')], 2.18 [m, 1H, H-C(2')], 1.05 [d, 6H, $^3J(H-C(3'), H-C(2'))$ = 6.5, H-C(3')]. ^{13}C NMR (100.6 MHz, DMSO- d_6): δ 143.9 [s, C(1)], 137.2 [s, C(4)], 126.0 [s, C(9)], 125.0 [s, C(10)], 124.7 [d, $^1J(C,H)$ = 155, C(7)], 124.6 [d, $^1J(C,H)$ = 162, C(6)], 122.7 [d, $^1J(C,H)$ = 129, C(8)], 122.2 [d, $^1J(C,H)$ = 127, C(5)], 109.3 [d, $^1J(C,H)$ = 153, C(2)], 105.0 [d, $^1J(C,H)$ = 159, C(3)], 56.1 [t, $^1J(C,H)$ = 140, C(1')], 26.4 [d, $^1J(C,H)$ = 155, C(2')], 11.0 [q, $^1J(C,H)$ = 127, C(3')]. ESI-TOF-HRMS: m/z calcd for (M + H) $C_{14}H_{18}NO$ 216.1388, found 216.1376.

(k) 4-(Pent-3-ylamino)-1-naphthol Hydrochloride (39). Product **39** was synthesized from 4-amino-1-naphthol hydrochloride and 3-pentanone according to the reductive amination procedure to afford a black solid in 92% yield. Mp: 135–138 °C dec. TLC: R_f = 0.55 (30% diethyl ether/pentane). 1H NMR (400 MHz, DMSO- d_6): δ 9.07 (bs, 1H, NH), 8.20 [d, 1H, $^3J(H-C(8), H-C(7))$ = 8.0, H-C(8)], 8.14 [d, 1H, $^3J(H-C(5), H-C(6))$ = 8.0, H-C(5)], 7.47–7.38 [m, 2H, H-C(6), H-C(7)], 6.78 [d, 1H, $^3J(H-C(2), H-C(3))$ = 8.0, H-C(2)], 6.41 [d, 1H, $^3J(H-C(3), H-C(2))$ = 8.0, H-C(3)], 4.90 (bs, 1H, OH), 3.28 [m, 1H, H-C(1')], 1.70–1.56 [m, 4H, H-C(2')], 1.02–0.90 [m, 6H, H-C(3')]. ^{13}C NMR (100.6 MHz, DMSO- d_6): δ 143.9 [s, C(1)], 137.2 [s, C(4)], 126.1 [s, C(9)], 125.0 [s, C(10)], 124.8 [d, $^1J(C,H)$ = 155, C(7)], 124.6 [d, $^1J(C,H)$ = 161, C(6)], 122.7 [d, $^1J(C,H)$ = 126, C(8)], 122.2 [d, $^1J(C,H)$ = 127, C(5)], 109.3 [d, $^1J(C,H)$ = 154, C(2)], 105.0 [d, $^1J(C,H)$ = 158, C(3)], 56.1 [t, $^1J(C,H)$ = 135, C(1')], 26.5 [t, $^1J(C,H)$ = 133, C(2')], 11.0 [dd, $^1J(C,H)$ = 125, C(3')]. ESI-TOF-HRMS: m/z calcd for (M) $C_{15}H_{19}NO$ 229.1467, found 229.1484.

(l) 4-(Cyclohexylamino)-1-naphthol Hydrochloride (40). Product **40** was synthesized from 4-amino-1-naphthol hydrochloride and cyclohexanone according to the reductive amination procedure to afford the hydrochloric salt as a white solid in 82% yield. Mp: 276–278 °C. TLC: R_f = 0.42 (40% diethyl ether/pentane). 1H NMR (400 MHz, DMSO- d_6 with D_2O): δ 8.47 [d, 1H, $^3J(H-C(8), H-C(7))$ = 8.5, H-C(8)], 8.19 [d, 1H, $^3J(H-C(5), H-C(6))$ = 8.5, H-C(5)], 7.78–7.64 [m, 4H, H-C(2), H-C(3), H-C(6), H-C(7)], 3.50 [m, 1H, H-C(1')], 2.15 [d, 2H, $^3J(H-C(2'), H-C(1'))$ = $^3J(H-C(6'), H-C(1'))$ = 8.5, H-C(2')-ax, H-C(6')-ax], 1.77 [d, 2H, $^3J(H-C(2'), H-C(1'))$ = $^3J(H-C(6'), H-C(1'))$ = 8.5, H-C(2')-eq, H-C(6')-eq], 1.68–1.54 [m, 2H, H-C(4')], 1.30–1.06 [m, 4H, H-C(3'), H-C(5')]. ^{13}C NMR (100.6 MHz, DMSO- d_6): δ 151.7 [s, C(1)], 128.2 [d, $^1J(C,H)$ = 156, C(7)], 127.2 [s, C(4)], 126.9 [d, $^1J(C,H)$ = 162, C(6)], 126.7 [s, C(9)], 126.6 [d, $^1J(C,H)$ = 129, C(8)], 124.0 [d, $^1J(C,H)$ = 128, C(5)], 121.9 [d, $^1J(C,H)$ = 156, C(2)], 121.9 [d, $^1J(C,H)$ = 156, C(3)], 117.0 [s, C(10)], 61.3 [d, $^1J(C,H)$ = 125, C(1')], 29.3 [t, $^1J(C,H)$ = 137, C(2'), C(6')], 25.0 [t, $^1J(C,H)$ = 137, C(3'), C(5')], 24.4 [t, $^1J(C,H)$ = 137, C(4')]. ESI-TOF-HRMS: m/z calcd for (M + H) $C_{16}H_{20}NO$ 242.1545, found 242.1544.

(m) 4-(Benzylamino)-1-naphthol Hydrochloride (41). Product **41** was synthesized from naphthalene-1,4-diol and benzylamine according to the nucleophilic addition procedure to afford a black solid in 65% yield. Mp: 102–105 °C. TLC: R_f = 0.47 (30% diethyl ether/pentane). 1H NMR (400 MHz, DMSO- d_6): δ 9.18 (bs, 1H, NH), 8.24 [d, 1H, $^3J(H-C(8), H-C(7))$ = 8.0, H-C(8)], 8.18 [d, 1H, $^3J(H-C(5), H-C(6))$ = 8.0, H-C(5)], 7.52–7.20 [m, 7H, H-C(6), H-C(7), 5(H-C(Ph))], 6.71 [d, 1H, $^3J(H-C(2), H-C(3))$ = 8.0, H-C(2)], 6.31 [d, 1H, $^3J(H-C(3),$

H-C(2)) = 8.0, H-C(3)], 6.26 (bs, 1H, OH), 4.47 [bs, 2H, H-C(1')]. ^{13}C NMR (100.6 MHz, DMSO- d_6): δ 144.5 [s, C(1)], 141.1 [s, C(2')], 137.0 [s, C(4)], 128.7 [d, $^1J(\text{C,H}) = 160$, C(4')], 128.7 [d, $^1J(\text{C,H}) = 162$, C(6')], 127.5 [d, $^1J(\text{C,H}) = 158$, C(3')], 127.5 [d, $^1J(\text{C,H}) = 164$, C(7')], 126.9 [d, $^1J(\text{C,H}) = 155$, C(5')], 125.9 [s, C(9)], 125.0 [s, C(10)], 124.9 [d, $^1J(\text{C,H}) = 161$, C(7)], 124.9 [d, $^1J(\text{C,H}) = 160$, C(6)], 122.8 [d, $^1J(\text{C,H}) = 156$, C(8)], 122.2 [d, $^1J(\text{C,H}) = 155$, C(5)], 109.0 [d, $^1J(\text{C,H}) = 156$, C(2)], 105.0 [d, $^1J(\text{C,H}) = 157$, C(3)], 47.7 [t, $^1J(\text{C,H}) = 136$, C(1')]. ESI-TOF-HRMS: m/z calcd for (M + H) $\text{C}_{17}\text{H}_{16}\text{NO}$ 250.1232, found 250.1224.

(n) ***N*-(4-Hydroxy-1-naphthyl)ethane-1,2-diaminium Chloride (42)**. Product **42** was synthesized from naphthalene-1,4-diol and *tert*-butyl 2-aminoethylcarbamate according to the nucleophilic addition procedure to afford a black amorphous solid in 77% yield (Boc-**42**). TLC: $R_f = 0.50$ (30% diethyl ether/pentane). Boc-**42** (0.10 mmol) was suspended in 2 mL of HCl solution (4.0 M in dioxane), and the mixture was stirred at ambient temperature for 15 min. Diethyl ether (20 mL) was added, and the resulting crystals were filtered and washed with diethyl ether to give the dihydrochloric ammonium salt in quantitative yield. ^1H NMR (400 MHz, DMSO- d_6 with CDCl_3): δ 8.62 (bs, 1H, NH), 8.32–8.22 [m, 2H, H-C(8), H-C(5)], 7.72 [d, 1H, $^3J(\text{H-C}(3), \text{H-C}(2)) = 8.5$, H-C(3)], 7.66 [t, 1H, $^3J(\text{H-C}(7), \text{H-C}(6)) = 8.0$, H-C(7)], 7.58 [t, 1H, $^3J(\text{H-C}(6), \text{H-C}(7)) = 8.0$, H-C(6)], 7.04 [d, 1H, $^3J(\text{H-C}(2), \text{H-C}(3)) = 8.5$, H-C(2)], 3.53 [m, 2H, H-C(1')], 3.42 [m, 2H, H-C(2')]. ^{13}C NMR (100.6 MHz, DMSO- d_6): δ 154.6 [s, C(1)], 128.1 [d, $^1J(\text{C,H}) = 157$, C(7)], 127.2 [s, C(4)], 126.3 [d, $^1J(\text{C,H}) = 160$, C(6)], 125.6 [s, C(9)], 123.5 [d, $^1J(\text{C,H}) = 128$, C(8)], 123.0 [s, C(10)], 122.0 [d, $^1J(\text{C,H}) = 130$, C(5)], 122.0 [d, $^1J(\text{C,H}) = 153$, C(2)], 107.4 [d, $^1J(\text{C,H}) = 153$, C(3)], 47.7 [t, $^1J(\text{C,H}) = 139$, C(1')], 35.8 [t, $^1J(\text{C,H}) = 136$, C(2')]. ESI-TOF-HRMS: m/z calcd for (M + H) $\text{C}_{12}\text{H}_{15}\text{N}_2\text{O}$ 203.1184, found 203.1189.

(o) ***N*-(4-Hydroxy-1-naphthyl)propane-1,3-diaminium Chloride (43)**. Product **43** was synthesized from naphthalene-1,4-diol and *tert*-butyl 3-aminopropylcarbamate according to the nucleophilic addition procedure to afford a black amorphous solid in 95% yield (Boc-**43**). TLC: $R_f = 0.51$ (30% diethyl ether/pentane). Boc-**43** (0.10 mmol) was suspended in 2 mL of HCl solution (4.0 M in dioxane), and the mixture was stirred at ambient temperature for 15 min. Diethyl ether (20 mL) was added, and the resulting crystals were filtered and washed with diethyl ether to give the dihydrochloric ammonium salt in quantitative yield. ^1H NMR (400 MHz, DMSO- d_6): δ 8.30–8.20 [m, 2H, H-C(8), H-C(5)], 7.74 [d, 1H, $^3J(\text{H-C}(3), \text{H-C}(2)) = 8.5$, H-C(3)], 7.67 [t, 1H, $^3J(\text{H-C}(7), \text{H-C}(6)) = 8.0$, H-C(7)], 7.57 [t, 1H, $^3J(\text{H-C}(6), \text{H-C}(7)) = 8.0$, H-C(6)], 7.05 [d, 1H, $^3J(\text{H-C}(2), \text{H-C}(3)) = 8.5$, H-C(2)], 3.49 [m, 2H, H-C(1')], 2.94 [m, 2H, H-C(3')], 2.18 [m, 2H, H-C(2')]. ^{13}C NMR (100.6 MHz, DMSO- d_6): δ 154.9 [s, C(1)], 128.0 [d, $^1J(\text{C,H}) = 155$, C(7)], 127.5 [s, C(4)], 126.1 [d, $^1J(\text{C,H}) = 160$, C(6)], 125.6 [s, C(9)], 123.5 [d, $^1J(\text{C,H}) = 125$, C(8)], 123.2 [d, $^1J(\text{C,H}) = 130$, C(5)], 122.7 [s, C(10)], 122.1 [d, $^1J(\text{C,H}) = 153$, C(2)], 107.4 [d, $^1J(\text{C,H}) = 150$, C(3)], 48.5 [t, $^1J(\text{C,H}) = 140$, C(1')], 36.6 [t, $^1J(\text{C,H}) = 135$, C(3')], 24.1 [t, $^1J(\text{C,H}) = 130$, C(2')]. ESI-TOF-HRMS: m/z calcd for (M + H) $\text{C}_{13}\text{H}_{17}\text{N}_2\text{O}$ 217.1335, found 217.1334.

(p) **4-[2-(Diethylamino)ethylamino]-1-naphthol Dihydrochloride (44)**. Product **44** was synthesized from naphthalene-1,4-diol and *N,N*-diethylethylenediamine according to the nucleophilic addition procedure to afford a black solid in 84% yield. Mp: 152–155 °C. TLC: $R_f = 0.45$ (30% diethyl ether/pentane). ^1H NMR (400 MHz, DMSO- d_6): δ 8.35 (bs, 1H, NH), 8.12 [m, 1H, $^3J(\text{H-C}(8), \text{H-C}(7)) = 8.0$, H-C(8)], 7.94 [d, 1H, $^3J(\text{H-C}(5), \text{H-C}(6)) = 8.0$, H-C(5)], 7.48–7.41 [m, 2H, H-C(6), H-C(7)], 6.76 [d, 1H, $^3J(\text{H-C}(2), \text{H-C}(3)) = 8.0$, H-C(2)], 6.40 [d, 1H, $^3J(\text{H-C}(3), \text{H-C}(2)) = 8.0$, H-C(3)], 5.20 (bs, 1H, OH), 3.16 [t, 2H, $^3J(\text{H-C}(1'), \text{H-C}(2')) = 6.5$, H-C(1')], 2.77 [t, 2H, $^3J(\text{H-C}(2'), \text{H-C}(1')) = 6.5$, H-C(2')], 2.57 [dd, 4H, $^2J = 12.5$, $^3J(\text{H-(CH}_2\text{)}, \text{H-(CH}_3\text{)}) = 6.5$, CH_2CH_3], 1.01 [t, 6H, $^3J(\text{H-(CH}_2\text{)}, \text{H-(CH}_3\text{)}) = 6.6$,

CH_2CH_3]. ^{13}C NMR (100.6 MHz, DMSO- d_6): δ 144.7 [s, C(1)], 137.3 [s, C(4)], 132.8 [s, C(9)], 125.9 [s, C(10)], 125.1 [d, $^1J(\text{C,H}) = 155$, C(7)], 124.9 [d, $^1J(\text{C,H}) = 129$, C(6)], 122.9 [d, $^1J(\text{C,H}) = 127$, C(8)], 121.5 [d, $^1J(\text{C,H}) = 153$, C(5)], 109.0 [d, $^1J(\text{C,H}) = 159$, C(2)], 104.7 [d, $^1J(\text{C,H}) = 159$, C(3)], 51.6 [t, $^1J(\text{C,H}) = 140$, C(1')], 47.1 [t, $^1J(\text{C,H}) = 135$, CH_2CH_3], 42.1 [t, $^1J(\text{C,H}) = 135$, C(2')], 12.2 [dd, $^1J(\text{C,H}) = 127$, CH_2CH_3]. ESI-TOF-HRMS: m/z calcd for (M + H) $\text{C}_{16}\text{H}_{23}\text{N}_2\text{O}$ 259.1810, found 259.1817.

(q) **2-Amino-*N*-(4-hydroxynaphth-1-yl)acetamide Hydrochloride (46)**. Product **46** was synthesized from TBS-protected 4-amino-1-naphthol hydrochloride and Boc-glycine according to the amino acid coupling procedure followed by deprotection from Boc to afford a white solid in 90% yield. Mp: 257–259 °C. TLC (Boc-protected): $R_f = 0.40$ (50% diethyl ether/pentane). ^1H NMR (400 MHz, DMSO- d_6): δ 10.48 (bs, 1H, NH), 8.45 [bs, 2H, NH_2], 8.15 [d, 1H, $^3J(\text{H-C}(8), \text{H-C}(7)) = 8.0$, H-C(8)], 7.99 [d, 1H, $^3J(\text{H-C}(5), \text{H-C}(6)) = 8.0$, H-C(5)], 7.55–7.42 [m, 2H, H-C(6), H-C(7)], 7.33 [d, 1H, $^3J(\text{H-C}(2), \text{H-C}(3)) = 8.0$, H-C(2)], 6.98 [d, 1H, $^3J(\text{H-C}(3), \text{H-C}(2)) = 8.0$, H-C(3)], 4.00–3.90 [m, 2H, H-C(2')], 3.79 (bs, 1H, OH). ^{13}C NMR (100.6 MHz, DMSO- d_6): δ 166.1 [s, C(1')], 152.3 [s, C(1)], 130.0 [s, C(4)], 126.6 [d, $^1J(\text{C,H}) = 128$, C(7)], 125.2 [s, C(9)], 125.2 [d, $^1J(\text{C,H}) = 160$, C(6)], 124.0 [s, C(10)], 123.9 [d, $^1J(\text{C,H}) = 128$, C(5)], 123.5 [d, $^1J(\text{C,H}) = 158$, C(8)], 122.7 [d, $^1J(\text{C,H}) = 127$, C(3)], 107.8 [d, $^1J(\text{C,H}) = 155$, C(2)], 41.1 [dd, $^1J(\text{C,H}) = 125$, C(2')]. ESI-TOF-HRMS: m/z calcd for (M + H) $\text{C}_{12}\text{H}_{13}\text{N}_2\text{O}_2$ 217.0977, found 217.0985.

(r) **(*S*)-2-Amino-*N*-(4-hydroxynaphth-1-yl)propanamide Hydrochloride (47)**. Product **47** was synthesized from TBS-protected 4-amino-1-naphthol hydrochloride and Boc-L-alanine according to the amino acid coupling procedure followed by deprotection from Boc to afford a white solid in 94% yield. TLC (Boc-protected): $R_f = 0.45$ (50% diethyl ether/pentane). ^1H NMR (400 MHz, DMSO- d_6): δ 10.48 (bs, 1H, NH), 8.45 (bs, 2H, NH_2), 8.15 [d, 1H, $^3J(\text{H-C}(8), \text{H-C}(7)) = 8.0$, H-C(8)], 7.99 [d, 1H, $^3J(\text{H-C}(5), \text{H-C}(6)) = 8.0$, H-C(5)], 7.55–7.42 [m, 2H, H-C(6), H-C(7)], 7.33 [d, 1H, $^3J(\text{H-C}(2), \text{H-C}(3)) = 8.0$, H-C(2)], 6.98 [d, 1H, $^3J(\text{H-C}(3), \text{H-C}(2)) = 8.0$, H-C(3)], 4.00–3.90 [m, H, H-C(2')], 3.19 (bs, 1H, OH), 1.62 [m, 3H, H-C(3')]. ^{13}C NMR (100.6 MHz, DMSO- d_6): δ 166.1 [s, C(1')], 152.3 [s, C(1)], 130.0 [s, C(4)], 126.6 [d, $^1J(\text{C,H}) = 128$, C(7)], 125.2 [s, C(9)], 125.2 [d, $^1J(\text{C,H}) = 160$, C(6)], 124.0 [s, C(10)], 123.9 [d, $^1J(\text{C,H}) = 128$, C(5)], 123.5 [d, $^1J(\text{C,H}) = 158$, C(8)], 122.7 [d, $^1J(\text{C,H}) = 127$, C(3)], 107.8 [d, $^1J(\text{C,H}) = 155$, C(2)], 49.1 [d, $^1J(\text{C,H}) = 155$, C(2')], 18.5 [dd, $^1J(\text{C,H}) = 125$, C(3')]. ESI-TOF-HRMS: m/z calcd for (M + H) $\text{C}_{13}\text{H}_{15}\text{N}_2\text{O}_2$ 231.1134, found 231.1139.

(s) **(*R*)-2-Amino-*N*-(4-hydroxynaphth-1-yl)propanamide Hydrochloride (48)**. Product **48** was synthesized from TBS-protected 4-amino-1-naphthol hydrochloride and Boc-D-alanine according to the amino acid coupling procedure and deprotection from Boc to afford a white solid in 93% yield. Mp: 193–195 °C. TLC (Boc-protected): $R_f = 0.45$ (50% diethyl ether/pentane). ^1H NMR (400 MHz, DMSO- d_6): δ 10.47 (bs, 1H, NH), 8.44 (bs, 2H, NH_2), 8.14 [d, 1H, $^3J(\text{H-C}(8), \text{H-C}(7)) = 8.0$, H-C(8)], 7.98 [d, 1H, $^3J(\text{H-C}(5), \text{H-C}(6)) = 8.0$, H-C(5)], 7.54–7.41 [m, 2H, H-C(6), H-C(7)], 7.32 [d, 1H, $^3J(\text{H-C}(2), \text{H-C}(3)) = 8.0$, H-C(2)], 6.97 [d, 1H, $^3J(\text{H-C}(3), \text{H-C}(2)) = 8.0$, H-C(3)], 3.99–3.89 [m, 1H, H-C(2')], 3.20 (bs, 1H, OH), 1.64 [m, 3H, H-C(3')]. ^{13}C NMR (100.6 MHz, DMSO- d_6): δ 166.2 [s, C(1')], 152.4 [s, C(1)], 130.1 [s, C(4)], 126.7 [d, $^1J(\text{C,H}) = 129$, C(7)], 125.3 [s, C(9)], 125.3 [d, $^1J(\text{C,H}) = 163$, C(6)], 124.1 [s, C(10)], 124.0 [d, $^1J(\text{C,H}) = 129$, C(5)], 123.6 [d, $^1J(\text{C,H}) = 160$, C(8)], 122.8 [d, $^1J(\text{C,H}) = 126$, C(3)], 107.9 [d, $^1J(\text{C,H}) = 153$, C(2)], 49.2 [dd, $^1J(\text{C,H}) = 155$, C(2')], 18.5 [dd, $^1J(\text{C,H}) = 125$, C(3')]. ESI-TOF-HRMS: m/z calcd for (M + H) $\text{C}_{13}\text{H}_{15}\text{N}_2\text{O}_2$ 231.1134, found 231.1139.

(t) **4-(2-Hydroxyethoxy)-1-naphthol (51)**. To a solution of 1,4-naphthoquinone (1 mg, 6.2 mmol) in toluene (2 mL) was added ethylene glycol (1.92 mg, 31 mmol). The mixture was refluxed for 1 h. After cooling, the mixture was diluted by addition of

50 mL of diethyl ether and 50 mL of water. The aqueous phase was extracted with diethyl ether (2 × 50 mL). The combined organic phases were dried and concentrated in vacuo. FC (9:1 pentane/diethyl ether mixture) gave **28** as a brown solid in quantitative yield. Mp: 88–90 °C. TLC: R_f = 0.66 (50% diethyl ether/pentane). ^1H NMR (400 MHz, DMSO- d_6): δ 9.64 (bs, 1H, OH), 8.25 [dd, 1H, $^3J(\text{H-C}(5), \text{H-C}(6))$ = 6.0, $^4J(\text{H-C}(5), \text{H-C}(7))$ = 3.5, H-C(5)], 8.16 [dd, 1H, $^3J(\text{H-C}(8), \text{H-C}(7))$ = 6.5, $^4J(\text{H-C}(8), \text{H-C}(6))$ = 3.0, H-C(8)], 7.50 [m, 1H, H-C(7)], 7.05 [m, 1H, H-C(6)], 6.81 [d, 1H, $^3J(\text{H-C}(2), \text{H-C}(3))$ = 8.5, H-C(2)], 6.78 [d, 1H, $^3J(\text{H-C}(3), \text{H-C}(2))$ = 8.5, H-C(3)], 5.02 (bs, 1H, OH), 4.06 [t, 2H, $^3J(\text{H-C}(1'), \text{H-C}(2'))$ = 5.0, H-C(1')], 3.87 [t, 2H, $^3J(\text{H-C}(2'), \text{H-C}(1'))$ = 5.0, H-C(2')]. ^{13}C NMR (100.6 MHz, DMSO- d_6): δ 147.5 [s, C(1)], 147.2 [s, C(4)], 127.5 [s, C(10)], 125.8 [s, C(9)], 125.7 [d, $^1J(\text{C}, \text{H})$ = 155, C(6)], 125.6 [d, $^1J(\text{C}, \text{H})$ = 162, C(7)], 122.4 [d, $^1J(\text{C}, \text{H})$ = 129, C(5)], 122.2 [d, $^1J(\text{C}, \text{H})$ = 127, C(8)], 107.7 [d, $^1J(\text{C}, \text{H})$ = 153, C(2)], 106.3 [d, $^1J(\text{C}, \text{H})$ = 159, C(3)], 70.1 [t, $^1J(\text{C}, \text{H})$ = 140, C(1')], 60.4 [t, $^1J(\text{C}, \text{H})$ = 140, C(2')]. ESI-TOF-HRMS: m/z calcd for (M) $\text{C}_{12}\text{H}_{12}\text{O}_3$ 204.0786, found 204.0782.

(u) **4-Methoxy-1-naphthylamine (52)**. 1-Methoxy-4-nitronaphthalene (1 mg, 4.9 mmol) was dissolved in 10 mL of methanol followed by addition of 80% hydrazine hydrate (1 mL). Raney nickel (0.3 mg) was carefully added before the mixture was refluxed. After completion of the reduction (1–2 h), which was marked by the disappearance of the yellow-orange color of the nitro compound, the catalyst was filtered out and methanol was removed under reduced pressure. The obtained crude 4-methoxynaphthalen-1-amine was converted to the corresponding hydrochloric salt via treatment of the amine in diethyl ether with dry hydrochloric acid in 2-propanol or dioxane. The formed precipitate was filtered, washed with diethyl ether, and recrystallized from an ethyl acetate/methanol mixture to give 0.95 mg of a white solid in 92% yield. Mp: 248–250 °C. ^1H NMR (400 MHz, DMSO- d_6): δ 8.16 [m, 1H, H-C(8)], 8.12 [m, 1H, H-C(5)], 7.50–7.45 [m, 2H, H-C(6), H-C(7)], 6.79 [d, 1H, $^3J(\text{H-C}(3), \text{H-C}(2))$ = 8.5, H-C(3)], 6.40 [d, 1H, $^3J(\text{H-C}(2), \text{H-C}(3))$ = 8.5, H-C(2)], 5.53 (bs, 2H, NH_2), 3.87 (s, 3H, OCH_3). ^{13}C NMR (100.6 MHz, DMSO- d_6): δ 146.7 [s, C(1)], 138.8 [s, C(4)], 126.2 [s, C(9)], 125.5 [d, $^1J(\text{C}, \text{H})$ = 160, C(6)], 125.2 [d, $^1J(\text{C}, \text{H})$ = 158, C(7)], 124.9 [s, C(10)], 122.4 [d, $^1J(\text{C}, \text{H})$ = 127, C(8)], 122.1 [d, $^1J(\text{C}, \text{H})$ = 128, C(5)], 105.8 [d, $^1J(\text{C}, \text{H})$ = 158, C(3)], 103.2 [d, $^1J(\text{C}, \text{H})$ = 155, C(2)], 55.9 [dd, $^1J(\text{C}, \text{H})$ = 125, OCH_3]. ESI-TOF-HRMS: m/z calcd for (M + H) $\text{C}_{11}\text{H}_{12}\text{NO}$ 174.0919, found 174.0925.

(v) **(4E,4'E)-4,4'-Bis(isopropylimino)-2,2'-binaphthyl-1,1'-(4H,4'H)-dione (53)**. Product **53** was synthesized from 4-(isopropylamino)-1-naphthol (**36**) according to the oxidation reaction with Ag_2O to afford a yellow amorphous solid in 45% yield. TLC: R_f = 0.69 (30% diethyl ether/pentane). ^1H NMR (400 MHz, DMSO- d_6): δ 8.48 [d, 2H, $^3J(\text{H-C}(8), \text{H-C}(7))$ = $^3J(\text{H-C}(8'), \text{H-C}(7'))$ = 8.0, H-C(8), H-C(8')], 8.19 [d, 2H, $^3J(\text{H-C}(5), \text{H-C}(6))$ = $^3J(\text{H-C}(5'), \text{H-C}(6'))$ = 7.5, H-C(5), H-C(5')], 7.77 [s, 2H, H-C(3), H-C(3')], 7.71 [t, 2H, $^3J(\text{H-C}(6), \text{H-C}(5))$ = $^3J(\text{H-C}(6'), \text{H-C}(5'))$ = 7.5, H-C(6), H-C(6')], 7.67 [t, 2H, $^3J(\text{H-C}(7), \text{H-C}(8))$ = $^3J(\text{H-C}(7'), \text{H-C}(8'))$ = 8.0, H-C(7), H-C(7')], 4.42 [m, 2H, $\text{CH}(\text{CH}_3)_2$], 1.40 [d, 12H, $^3J(\text{CH}(\text{CH}_3)_2, \text{CH}(\text{CH}_3)_2)$ = 6.0, $\text{CH}(\text{CH}_3)_2$]. ^{13}C NMR (100.6 MHz, DMSO- d_6): δ 184.0 [s, C(1), C(1')], 152.1 [s, C(4), C(4')], 137.0 [s, C(9), C(9')], 135.9 [s, C(10), C(10')], 133.1 [d, $^1J(\text{C}, \text{H})$ = 161, C(7), C(7')], 131.1 [s, C(2), C(2')], 130.3 [d, $^1J(\text{C}, \text{H})$ = 162, C(6), C(6')], 127.3 [d, $^1J(\text{C}, \text{H})$ = 163, C(5), C(5')], 126.3 [d, $^1J(\text{C}, \text{H})$ = 165, C(8), C(8')], 124.5 [d, $^1J(\text{C}, \text{H})$ = 164, C(3), C(3')], 51.9 [t, $^1J(\text{C}, \text{H})$ = 132, $\text{CH}(\text{CH}_3)_2$], 24.5 [q, $^1J(\text{C}, \text{H})$ = 127, $\text{CH}(\text{CH}_3)_2$]. ESI-TOF-HRMS: m/z calcd for (M + H) $\text{C}_{26}\text{H}_{25}\text{N}_2\text{O}_2$ 397.1916, found 397.1930.

(w) **(4E,4'E)-4,4'-Bis(pentan-3-ylimino)-2,2'-binaphthyl-1,1'-(4H,4'H)-dione (54)**. Product **54** was synthesized from 4-(pentan-3-ylamino)-1-naphthol (**39**) according to the oxidation reaction with Ag_2O to afford a yellow amorphous solid in 56% yield.

TLC: R_f = 0.75 (30% diethyl ether/pentane). ^1H NMR (400 MHz, DMSO- d_6): δ 8.53 [d, 2H, $^3J(\text{H-C}(8), \text{H-C}(7))$ = $^3J(\text{H-C}(8'), \text{H-C}(7'))$ = 7.0, H-C(8), H-C(8')], 8.24 [d, 2H, $^3J(\text{H-C}(5), \text{H-C}(6))$ = $^3J(\text{H-C}(5'), \text{H-C}(6'))$ = 7.0, H-C(5), H-C(5')], 7.80 [s, 2H, H-C(3), H-C(3')], 7.73 [t, 2H, $^3J(\text{H-C}(6), \text{H-C}(5))$ = $^3J(\text{H-C}(6'), \text{H-C}(5'))$ = 7.0, H-C(6), H-C(6')], 7.64 [t, 2H, $^3J(\text{H-C}(7), \text{H-C}(8))$ = $^3J(\text{H-C}(7'), \text{H-C}(8'))$ = 7.0, H-C(7), H-C(7')], 3.95 [m, 2H, $\text{CH}(\text{CH}_2\text{CH}_3)_2$], 1.84 [m, 2H, $\text{CH}(\text{CH}_2\text{CH}_3)_2$], 0.94 [t, 12H, $^3J(\text{CH}(\text{CH}_2\text{CH}_3)_2, \text{CH}(\text{CH}_2\text{CH}_3)_2)$ = 6.0, $\text{CH}(\text{CH}_2\text{CH}_3)_2$]. ^{13}C NMR (100.6 MHz, DMSO- d_6): δ 184.1 [s, C(1), C(1')], 153.3 [s, C(4), C(4')], 139.0 [s, C(9), C(9')], 135.9 [s, C(10), C(10')], 133.1 [d, $^1J(\text{C}, \text{H})$ = 161, C(7), C(7')], 131.1 [s, C(2), C(2')], 130.3 [d, $^1J(\text{C}, \text{H})$ = 162, C(6), C(6')], 127.6 [d, $^1J(\text{C}, \text{H})$ = 163, C(5), C(5')], 126.4 [d, $^1J(\text{C}, \text{H})$ = 165, C(8), C(8')], 124.6 [d, $^1J(\text{C}, \text{H})$ = 164, C(3), C(3')], 64.1 [d, $^1J(\text{C}, \text{H})$ = 132, $\text{CH}(\text{CH}_2\text{CH}_3)_2$], 29.5 [t, $^1J(\text{C}, \text{H})$ = 132, $\text{CH}(\text{CH}_2\text{CH}_3)_2$], 11.1 [q, $^1J(\text{C}, \text{H})$ = 127, $\text{CH}(\text{CH}_2\text{CH}_3)_2$]. ESI-TOF-HRMS: m/z calcd for (M + H) $\text{C}_{30}\text{H}_{33}\text{N}_2\text{O}_2$ 453.2542, found 453.2534.

(x) **(E)-4-(Isopropylimino)-2-methylnaphthalen-1(4H)-one (55)**. Product **55** was synthesized from vitamin K5 and acetone according to the reductive amination procedure followed by the oxidation reaction with Ag_2O to afford a yellow amorphous solid in 61% yield. TLC: R_f = 0.65 (30% diethyl ether/pentane). ^1H NMR (400 MHz, CDCl_3): δ 8.40 [dd, 1H, $^3J(\text{H-C}(8), \text{H-C}(7))$ = 8.0, $^4J(\text{H-C}(8), \text{H-C}(6))$ = 1.5, H-C(8)], 8.11 [dd, 1H, $^3J(\text{H-C}(5), \text{H-C}(6))$ = 8.0, $^4J(\text{H-C}(5), \text{H-C}(7))$ = 1.5, H-C(5)], 7.62 [dt, 1H, $^3J(\text{H-C}(7), \text{H-C}(8))$ = 8.0, $^3J(\text{H-C}(7), \text{H-C}(6))$ = 8.0, $^4J(\text{H-C}(7), \text{H-C}(5))$ = 1.5, H-C(6)], 7.55 [dt, 1H, $^3J(\text{H-C}(6), \text{H-C}(5))$ = 8.0, $^3J(\text{H-C}(6), \text{H-C}(7))$ = 8.0, $^4J(\text{H-C}(6), \text{H-C}(8))$ = 1.5, H-C(6)], 7.38 [bs, 1H, H-C(3)], 4.32 [m, 1H, $\text{NCH}(\text{CH}_3)_2$], 2.18 [s, 3H, C(2) CH_3], 1.33 [d, 6H, $^3J(\text{NCH}(\text{CH}_3)_2, \text{NCH}(\text{CH}_3)_2)$ = 6.5, $\text{NCH}(\text{CH}_3)_2$]. ^{13}C NMR (100.6 MHz, DMSO- d_6): δ 186.1 [s, C(1)], 152.4 [s, C(4)], 141.0 [s, C(10)], 136.3 [s, C(2)], 132.5 [d, $^1J(\text{C}, \text{H})$ = 161, C(3)], 131.0 [s, C(9)], 129.9 [d, $^1J(\text{C}, \text{H})$ = 162, C(6)], 125.8 [d, $^1J(\text{C}, \text{H})$ = 160, C(7)], 124.5 [d, $^1J(\text{C}, \text{H})$ = 165, C(8)], 124.2 [d, $^1J(\text{C}, \text{H})$ = 163, C(5)], 51.2 [t, $^1J(\text{C}, \text{H})$ = 132, $\text{NCH}(\text{CH}_3)_2$], 24.4 [q, $^1J(\text{C}, \text{H})$ = 127, $\text{NCH}(\text{CH}_3)_2$], 17.0 [q, $^1J(\text{C}, \text{H})$ = 125, C(2) CH_3]. ESI-TOF-HRMS: m/z calcd for (M + H) $\text{C}_{14}\text{H}_{16}\text{NO}$ 214.1232, found 214.1224.

Protein Expression and Purification of Recombinant Human IDO. The coding region for human IDO (Ala2–Gly403) was cloned into a derivative of plasmid pET9 (Novagen). The recombinant plasmid, pETIDO, encodes a histidine tag at the N-terminus of IDO. Bacterial strain BL21 AI (Invitrogen) was used for overexpression of IDO and transformed with the pETIDO plasmid. The transformed cells were grown on a rotary shaker at 37 °C and 220 rpm to an OD_{600} of 1.2, in LB medium supplemented with 25 $\mu\text{g}/\text{mL}$ kanamycin, 50 $\mu\text{g}/\text{mL}$ L-tryptophan and 10 μM bovine hemin (Sigma). The culture was cooled in a water/ice bath and supplemented again with 50 $\mu\text{g}/\text{mL}$ L-tryptophan and 10 μM bovine hemin. The expression of His-tagged IDO was induced by the addition of 1% (w/v) arabinose. Induced cells were grown at 20 °C and 60 rpm for 20 h. Cells (1 L culture) were collected by centrifugation, resuspended in 40 mL of 25 mM Mes, 150 mM KCl, 10 mM imidazole, and protease inhibitors (complete EDTA free, Roche Applied Science) (pH 6.5), and disrupted with a French press. The extract was clarified by centrifugation and filtration on a 0.22 μm filter. The enzyme was purified by IMAC using Ni^{2+} as a ligand and an IMAC HITRAP column (5 mL, GE Healthcare). Briefly, the extract was loaded on the column with 25 mM Mes, 150 mM KCl, and 10 mM imidazole (pH 6.5). The column was washed with 50 mL of the same buffer with the imidazole concentration adjusted to 100 mM. Finally, the protein was eluted with 25 mM Mes, 150 mM KCl, and 50 mM EDTA (pH 6.5). The buffer was then exchanged into 25 mM Mes and 150 mM KCl (pH 6.5) using a HITRAP desalting column (GE Healthcare). The purity of the enzyme was estimated to be >95% based on the SDS–PAGE gel and Coomassie blue staining. The ratio of absorbance at 404 nm to that at 280 nm of the protein was around 1.9.

Enzymatic Assay. The enzymatic inhibition assays were performed as described by Takikawa et al.⁸⁷ with some modifications. Briefly, the reaction mixture (100 μ L) contained potassium phosphate buffer (100 mM, pH 6.5) ascorbic acid (20 mM), catalase (200 units/mL), methylene blue (10 μ M), purified recombinant IDO (2 ng/ μ L), L-Trp (200 μ M), and DMSO (5 μ L). The inhibitors were serially diluted 10-fold from 1000 to 0.1 μ M or, if not soluble at 1000 μ M, by 4 orders of magnitude from their highest soluble concentration. The reaction was conducted at 37 °C for 60 min and stopped by addition of 30% (w/v) trichloroacetic acid (40 μ L). To convert *N*-formylkynurenine to kynurenine, the tubes were incubated at 50 °C for 30 min, followed by centrifugation at 10000g for 20 min. Lastly, 100 μ L of supernatant from each probe was transferred to another tube for HPLC analysis. The mobile phase for HPLC measurements consisted of 50% sodium citrate buffer (40 mM, pH 2.25) and 50% methanol with 400 μ M SDS. The rate of flow through the S5-ODS1 column was 1 mL/min, and kynurenine was detected at a wavelength of 365 nm.

A compound was defined as "active" when it showed a clear signal on the dose–response curve. The following classification of IDO inhibitory activity is used in the text: very weak ($IC_{50} > 1000$ μ M), weak ($IC_{50} = 100$ – 1000 μ M), moderate ($IC_{50} = 10$ – 100 μ M), and strong ($IC_{50} = 0.1$ – 10 μ M).

Cellular Assay. (i) **Cell Lines.** A plasmid construct encoding murine IDO was transfected into mouse mastocytoma line P815B. Clone P815B-mIDO clone 6,⁷ which overexpresses IDO, was selected and used for the cellular assay. Mouse IDO shares a 62% sequence identity with human IDO,⁸⁸ and the active site residues mentioned in the Introduction are 100% conserved. For the assays evaluating inhibition of human IDO, a plasmid construct encoding human IDO was transfected into human HEK-293 cells, and clone 293-hIDO clone 17⁷ was selected and used in the assay. For the assays evaluating inhibition of mouse TDO, a plasmid construct encoding murine TDO was transfected into mouse mastocytoma cell line P815B. Clone P815B-mTDO clone 12, which overexpresses TDO, was selected and used for the cellular assay. Mouse TDO shares 88% sequence identity and a 7% sequence homology with human TDO, and the active site residues are 100% conserved.⁸⁹

(ii) **Assay.** The assay was performed in 96-well flat bottom plates seeded with 2×10^5 cells in a final volume of 200 μ L. To determine whether compounds were significant IDO or TDO inhibitors, the cells were incubated overnight at 37 °C in HBSS (Hank's Balanced Salt Solution, Invitrogen) supplemented with 50 μ M L-Trp and the compound at 2, 20, or 200 μ M. To determine the IC_{50} , the cells were incubated for 8 h at 37 °C in HBSS supplemented with 80 μ M L-tryptophan and a titration of the compound ranging from 0.312 to 80 μ M (**1**, **12**, and **29**) or from 1.56 to 400 μ M (**15**, **34**, **36**, and L-IMT). The plates were then centrifuged for 10 min at 300g, and 150 μ L of the supernatant were collected. The supernatant was analyzed by HPLC to measure the concentration of tryptophan and kynurenine. For HPLC analysis, 50 μ L of supernatant was mixed with 500 μ L of acetonitrile to precipitate the proteins. After centrifugation, the supernatant was collected, concentrated on a speedvac, resuspended in a final volume of 100 μ L of water, and injected into the HPLC system (C18 column). Trp was detected at an absorption wavelength of 280 nm, and kynurenine at 360 nm. Under the conditions used for IC_{50} estimation, ~50% of the initial amount of tryptophan was degraded in the absence of inhibitor, and an equimolar amount of kynurenine was produced. The percentages of inhibition of tryptophan degradation and kynurenine production by the compounds were calculated in reference to this maximal activity. The initial wells containing the cells in the remaining volume of 50 μ L were used to estimate cell viability in a classical MTT assay. To that end, 50 μ L of culture medium (Isocove medium with 10% FCS and amino acids) was added to the wells together with 50 μ L of MTT. After incubation for 3–4 h at 37 °C, 100 μ L of SDS/DMF was added

to dissolve the crystals of formazan blue. The ratio of absorbance at 570 nm to that at 650 nm was measured after overnight incubation at 37 °C.

Acknowledgment. We are much obliged to the Center of Integrative Genomics (University of Lausanne), especially to Gilles Boss and Sylvian Bron, for assistance with the enzymatic assay. For computational resources and support, we thank the Vital-IT team at the Swiss Institute for Bioinformatics. We thank Luc Pilotte for help in setting up and running the cellular assay. This work was supported by SCORE funds (3232B0-103172 and 3200B0-103173) to O.M. from the Swiss National Science Foundation, by the Clinical Discovery Program of the Ludwig Institute for Cancer Research and the Atlantic Philanthropies, and by CANTOL, a project of BioWin, the Health Cluster of Wallonia. Molecular graphics images were produced using the UCSF Chimera package from the Resource for Biocomputing, Visualization, and Informatics at the University of California, San Francisco (supported by National Institutes of Health Grant P41 RR-01081).⁹⁰ Instant JChem was used for structure database management and search, Instant JChem 2.3, 2008, ChemAxon (<http://www.chemaxon.com>). Marvin was used for drawing, displaying, and characterizing chemical structures, Marvin 5.0.3, 2008, ChemAxon (<http://www.chemaxon.com>). We thank Michel Cuendet for helpful discussions.

Supporting Information Available: Coordinates of docked conformations of 134 known IDO inhibitors (pdb/dock4 format, for use with X-ray structure 2D0T, chain A); ¹H, ¹³C, and DEPT ¹³C NMR spectra for compounds **31**, **32**, **34**–**36**, **38**–**41**, **Boc-42**, **42**, **Boc-43**, **43**, **44**, **46**–**48**, and **51**–**55**; results of DFT calculations for compound **1**; structures of 65 docked FDA-approved compounds; structures of frameworks and side chains used for FBDD; and dose–response curves of all active compounds in enzymatic and cellular assays. This material is available free of charge via the Internet at <http://pubs.acs.org>.

References

- (1) Zamanakou, M.; Germenis, A. E.; Karanikas, V. Tumor immune escape mediated by indoleamine 2,3-dioxygenase. *Immunol. Lett.* **2007**, *111*, 69–75.
- (2) Katz, J. B.; Muller, A. J.; Prendergast, G. C. Indoleamine 2,3-dioxygenase in T-cell tolerance and tumoral immune escape. *Immunol. Rev.* **2008**, *222*, 206–221.
- (3) Prendergast, G. C. Immune escape as a fundamental trait of cancer: focus on IDO. *Oncogene* **2008**, *27*, 3889–3900.
- (4) Yamamoto, S.; Hayaishi, O. Tryptophan pyrrolase of rabbit intestine. D- and L-tryptophan-cleaving enzyme or enzymes. *J. Biol. Chem.* **1967**, *242*, 5260–5266.
- (5) Sono, M.; Roach, M.; Coulter, E.; Dawson, J. Heme-containing oxygenases. *Chem. Rev.* **1996**, *96*, 2841–2888.
- (6) Hwu, P.; Du, M. X.; Lapointe, R.; Do, M.; Taylor, M. W.; Young, H. A. Indoleamine 2,3-dioxygenase production by human dendritic cells results in the inhibition of T cell proliferation. *J. Immunol.* **2000**, *164*, 3596–3599.
- (7) Uyttenhove, C.; Pilotte, L.; Théate, I.; Stroobant, V.; Colau, D.; Parmentier, N.; Boon, T.; Van den Eynde, B. J. Evidence for a tumoral immune resistance mechanism based on tryptophan degradation by indoleamine 2,3-dioxygenase. *Nat. Med.* **2003**, *9*, 1269–1274.
- (8) Okamoto, A.; Nikaido, T.; Ochiai, K.; Takakura, S.; Saito, M.; Aoki, Y.; Ishii, N.; Yanaihara, N.; Yamada, K.; Takikawa, O.; Kawaguchi, R.; Isonishi, S.; Tanaka, T.; Urashima, M. Indoleamine 2,3-dioxygenase serves as a marker of poor prognosis in gene expression profiles of serous ovarian cancer cells. *Clin. Cancer Res.* **2005**, *11*, 6030–6039.
- (9) Brandacher, G.; Perathoner, A.; Ladurner, R.; Schneeberger, S.; Obrist, P.; Winkler, C.; Werner, E. R.; Werner-Felmayer, G.; Weiss, H. G.; Göbel, G.; Margreiter, R.; Königsrainer, A.; Fuchs, D.; Amberger, A. Prognostic value of indoleamine 2,3-dioxygenase

- expression in colorectal cancer: Effect on tumor-infiltrating T cells. *Clin. Cancer Res.* **2006**, *12*, 1144–1151.
- (10) Ino, K.; Yoshida, N.; Kajiyama, H.; Shibata, K.; Yamamoto, E.; Kidokoro, K.; Takahashi, N.; Terauchi, M.; Nawa, A.; Nomura, S.; Nagasaka, T.; Takikawa, O.; Kikkawa, F. Indoleamine 2,3-dioxygenase is a novel prognostic indicator for endometrial cancer. *Br. J. Cancer* **2006**, *95*, 1555–1561.
 - (11) Pan, K.; Wang, H.; Chen, M.-S.; Zhang, H.-K.; Weng, D.-S.; Zhou, J.; Huang, W.; Li, J.-J.; Song, H.-F.; Xia, J.-C. Expression and prognosis role of indoleamine 2,3-dioxygenase in hepatocellular carcinoma. *J. Cancer Res. Clin. Oncol.* **2008**, *134*, 1247–1253.
 - (12) Muller, A. J.; DuHadaway, J. B.; Donovan, P. S.; Sutanto-Ward, E.; Prendergast, G. C. Inhibition of indoleamine 2,3-dioxygenase, an immunoregulatory target of the cancer suppression gene Bin1, potentiates cancer chemotherapy. *Nat. Med.* **2005**, *11*, 312–319.
 - (13) Shimizu, T.; Nomiya, S.; Hirata, F.; Hayaishi, O. Indoleamine 2,3-dioxygenase. Purification and some properties. *J. Biol. Chem.* **1978**, *253*, 4700–4706.
 - (14) Sugimoto, H.; Oda, S.; Otsuki, T.; Hino, T.; Yoshida, T.; Shiro, Y. Crystal structure of human indoleamine 2,3-dioxygenase: Catalytic mechanism of O₂ incorporation by a heme-containing dioxygenase. *Proc. Natl. Acad. Sci. U.S.A.* **2006**, *103*, 2611–2616.
 - (15) Chauhan, N.; Basran, J.; Efimov, I.; Svistunenko, D. A.; Seward, H. E.; Moody, P. C. E.; Raven, E. L. The role of serine 167 in human indoleamine 2,3-dioxygenase: A comparison with tryptophan 2,3-dioxygenase. *Biochemistry* **2008**, *47*, 4761–4769.
 - (16) Chauhan, N.; Thackray, S. J.; Rafice, S. A.; Eaton, G.; Lee, M.; Efimov, I.; Basran, J.; Jenkins, P. R.; Mowat, C. G.; Chapman, S. K.; Raven, E. L. Reassessment of the reaction mechanism in the heme dioxygenases. *J. Am. Chem. Soc.* **2009**, *131*, 4186–4187.
 - (17) Vottero, E.; Mitchell, D. A.; Page, M. J.; MacGillivray, R. T. A.; Sadowski, I. J.; Roberge, M.; Mauk, A. G. Cytochrome b₅ is a major reductant in vivo of human indoleamine 2,3-dioxygenase expressed in yeast. *FEBS Lett.* **2006**, *580*, 2265–2268.
 - (18) Maghzal, G. J.; Thomas, S. R.; Hunt, N. H.; Stocker, R. Cytochrome b₅, not superoxide anion radical, is a major reductant of indoleamine 2,3-dioxygenase in human cells. *J. Biol. Chem.* **2008**, *283*, 12014–12025.
 - (19) Watanabe, Y.; Fujiwara, M.; Hayaishi, O. 2,5-Dihydro-L-phenylalanine: A competitive inhibitor of indoleamine 2,3-dioxygenase. *Biochem. Biophys. Res. Commun.* **1978**, *85*, 273–279.
 - (20) Eguchi, N.; Watanabe, Y.; Kawanishi, K.; Hashimoto, Y.; Hayaishi, O. Inhibition of indoleamine 2,3-dioxygenase and tryptophan 2,3-dioxygenase by β -carbolines and indole derivatives. *Arch. Biochem. Biophys.* **1984**, *232*, 602–609.
 - (21) Sono, M.; Cady, S. G. Enzyme kinetic and spectroscopic studies of inhibitor and effector interactions with indoleamine 2,3-dioxygenase. 1. Norharman and 4-phenylimidazole binding to the enzyme as inhibitors and heme ligands. *Biochemistry* **1989**, *28*, 5392–5399.
 - (22) Cady, S. G.; Sono, M. 1-Methyl-DL-tryptophan, β -(3-benzofuran-2-yl)-DL-alanine (the oxygen analog of tryptophan), and β -(3-benzothienyl)-DL-alanine (the sulfur analog of tryptophan) are competitive inhibitors for indoleamine 2,3-dioxygenase. *Arch. Biochem. Biophys.* **1991**, *291*, 326–333.
 - (23) Peterson, A. C.; Loggia, A. J. L.; Hamaker, L. K.; Arend, R. A.; Fiset, P. L.; Okazi, Y.; Will, J. A.; Brown, R. R.; Cook, J. M. Evaluation of substituted β -carbolines as non-competitive indoleamine 2,3-dioxygenase inhibitors. *Med. Chem. Res.* **1993**, *3*, 473–482.
 - (24) Peterson, A. C.; Migawa, M. T.; Martin, M. J.; Hamaker, L. K.; Czerwinski, K. M.; Zhang, W.; Arend, R. A.; Fiset, P. L.; Okazi, Y.; Will, J. A.; Brown, R. R.; Cook, J. M. Evaluation of functionalized tryptophan derivatives and related compounds as competitive inhibitors of indoleamine 2,3-dioxygenase. *Med. Chem. Res.* **1994**, *3*, 531–544.
 - (25) Southan, M.; Truscott, R.; Jamie, J.; Pelosi, L.; Walker, M.; Maeda, H.; Iwamoto, Y.; Toné, S. Structural requirements of the competitive binding site of recombinant human indoleamine 2,3-dioxygenase. *Med. Chem. Res.* **1996**, *6*, 343–352.
 - (26) Andersen, R.; Pereira, A.; Huang, X.-H.; Mauk, G.; Vottero, E.; Roberge, M.; Balgi, A. Indoleamine 2,3-Dioxygenase (IDO) Inhibitors. Patent WO 2006/005185, **2006**.
 - (27) Brastianos, H. C.; Vottero, E.; Patrick, B. O.; Soest, R. V.; Maitanaho, T.; Mauk, A. G.; Andersen, R. J. Exiguamine A, an indoleamine-2,3-dioxygenase (IDO) inhibitor isolated from the marine sponge *Neopetrosia exigua*. *J. Am. Chem. Soc.* **2006**, *128*, 16046–16047.
 - (28) Pereira, A.; Vottero, E.; Roberge, M.; Mauk, A. G.; Andersen, R. J. Indoleamine 2,3-dioxygenase inhibitors from the northeastern Pacific marine hydroid *Garveia annulata*. *J. Nat. Prod.* **2006**, *69*, 1496–1499.
 - (29) Vottero, E.; Balgi, A.; Woods, K.; Tugendreich, S.; Melese, T.; Andersen, R. J.; Mauk, A. G.; Roberge, M. Inhibitors of human indoleamine 2,3-dioxygenase identified with a target-based screen in yeast. *Biotechnol. J.* **2006**, *1*, 282–288.
 - (30) Holbeck, S. L. Update on NCI in vitro drug screen utilities. *Eur. J. Cancer* **2004**, *40*, 785–793.
 - (31) Gaspari, P.; Banerjee, T.; Malachowski, W. P.; Muller, A. J.; Prendergast, G. C.; DuHadaway, J.; Bennett, S.; Donovan, A. M. Structure-activity study of brassinin derivatives as indoleamine 2,3-dioxygenase inhibitors. *J. Med. Chem.* **2006**, *49*, 684–692.
 - (32) Andersen, R.; Leblanc, M.; Brastianos, H.; Vottero, E.; Roberge, M.; Mauk, G.; Carr, G. Substituted Quinone Indoleamine 2,3-Dioxygenase (IDO) Inhibitors and Synthesis and Uses Thereof. Patent WO 2008/052352, **2008**.
 - (33) Carr, G.; Chung, M. K. W.; Mauk, A. G.; Andersen, R. J. Synthesis of indoleamine 2,3-dioxygenase inhibitory analogues of the sponge alkaloid exigamine A. *J. Med. Chem.* **2008**, *51*, 2634–2637.
 - (34) Kumar, S.; Malachowski, W.; DuHadaway, J.; Lalonde, J.; Carroll, P.; Jaller, D.; Metz, R.; Prendergast, G.; Muller, A. Indoleamine 2,3-dioxygenase is the anticancer target for a novel series of potent naphthoquinone-based inhibitors. *J. Med. Chem.* **2008**, *51*, 1706–1718.
 - (35) Kumar, S.; Jaller, D.; Patel, B.; LaLonde, J. M.; DuHadaway, J. B.; Malachowski, W. P.; Prendergast, G. C.; Muller, A. J. Structure based development of phenylimidazole-derived inhibitors of indoleamine 2,3-dioxygenase. *J. Med. Chem.* **2008**, *51*, 4968–4977.
 - (36) Nakashima, H.; Uto, Y.; Nakata, E.; Nagasawa, H.; Ikkyu, K.; Hiraoka, N.; Nakashima, K.; Sasaki, Y.; Sugimoto, H.; Shiro, Y.; Hashimoto, T.; Okamoto, Y.; Asakawa, Y.; Hori, H. Synthesis and biological activity of 1-methyl-tryptophan-tirapazamine hybrids as hypoxia-targeting indoleamine 2,3-dioxygenase inhibitors. *Bioorg. Med. Chem.* **2008**, *16*, 8661–8669.
 - (37) Carr, G.; Tay, W.; Bottrill, H.; Andersen, S. K.; Mauk, A. G.; Andersen, R. J. Plectosphaeric acids A, B, and C, indoleamine 2,3-dioxygenase inhibitors produced in culture by a marine isolate of the fungus *Plectosphaerella cucumerina*. *Org. Lett.* **2009**, *11*, 2996–2999.
 - (38) Combs, A.; Zhu, W.; Sparks, R. B. N-Hydroxyamidinoheterocycles as modulators of indoleamine 2,3-Dioxygenase. Patent WO 2008/058178, **2008**.
 - (39) Yue, E. W.; et al. Discovery of potent competitive inhibitors of indoleamine 2,3-dioxygenase with in vivo pharmacodynamic activity and efficacy in a mouse melanoma model. *J. Med. Chem.* **2009**, *52*, 7364–7367.
 - (40) Hou, D.-Y.; Muller, A. J.; Sharma, M. D.; DuHadaway, J.; Banerjee, T.; Johnson, M.; Mellor, A. L.; Prendergast, G. C.; Munn, D. H. Inhibition of indoleamine 2,3-dioxygenase in dendritic cells by stereoisomers of 1-methyl-tryptophan correlates with antitumor responses. *Cancer Res.* **2007**, *67*, 792–801.
 - (41) Metz, R.; DuHadaway, J. B.; Kamasani, U.; Laury-Kleintop, L.; Muller, A. J.; Prendergast, G. C. Novel tryptophan catabolic enzyme IDO2 is the preferred biochemical target of the antitumor indoleamine 2,3-dioxygenase inhibitory compound D-1-methyl-tryptophan. *Cancer Res.* **2007**, *67*, 7082–7087.
 - (42) Löb, S.; Königsrainer, A. Is IDO a key enzyme bridging the gap between tumor escape and tolerance induction? *Langenbecks Arch. Chir.* **2008**, *393*, 995–1003.
 - (43) Lob, S.; Königsrainer, A.; Schafer, R.; Rammensee, H.-G.; Opelz, G.; Terness, P. Levo-but not dextro-1-methyl tryptophan abrogates the IDO activity of human dendritic cells. *Blood* **2008**, *111*, 2152–2154.
 - (44) Löb, S.; Königsrainer, A.; Rammensee, H.-G.; Opelz, G.; Terness, P. Inhibitors of indoleamine-2,3-dioxygenase for cancer therapy: Can we see the wood for the trees? *Nat. Rev. Cancer* **2009**, *9*, 445–452.
 - (45) Grosdidier, A.; Zoete, V.; Michielin, O. EADock: Docking of small molecules into protein active sites with a multiobjective evolutionary optimization. *Proteins* **2007**, *67*, 1010–1025.
 - (46) Grosdidier, A.; Zoete, V.; Michielin, O. Blind docking of 260 protein-ligand complexes with EADock 2.0. *J. Comput. Chem.* **2009**, *30*, 2021–2030.
 - (47) Distributed Structure-Searchable Toxicity (DSSTox) (<http://epa.gov/ncet/dsstox/>), U.S. Environmental Protection Agency, **2009**.
 - (48) Rees, D. C.; Congreve, M.; Murray, C. W.; Carr, R. Fragment-based lead discovery. *Nat. Rev. Drug Discovery* **2004**, *3*, 660–672.
 - (49) Zartler, E. R.; Shapiro, M. J. Fragonomics: Fragment-based drug discovery. *Curr. Opin. Chem. Biol.* **2005**, *9*, 366–370.
 - (50) Hajduk, P. J.; Greer, J. A decade of fragment-based drug design: Strategic advances and lessons learned. *Nat. Rev. Drug Discovery* **2007**, *6*, 211–219.

- (51) Congreve, M.; Chessari, G.; Tisi, D.; Woodhead, A. J. Recent developments in fragment-based drug discovery. *J. Med. Chem.* **2008**, *51*, 3661–3680.
- (52) Hopkins, A. L.; Groom, C. R.; Alex, A. Ligand efficiency: A useful metric for lead selection. *Drug Discovery Today* **2004**, *9*, 430–431.
- (53) Carr, R. A. E.; Congreve, M.; Murray, C. W.; Rees, D. C. Fragment-based lead discovery: Leads by design. *Drug Discovery Today* **2005**, *10*, 987–992.
- (54) Bemis, G. W.; Murcko, M. A. The properties of known drugs. 1. Molecular frameworks. *J. Med. Chem.* **1996**, *39*, 2887–2893.
- (55) Bemis, G. W.; Murcko, M. A. Properties of known drugs. 2. Side chains. *J. Med. Chem.* **1999**, *42*, 5095–5099.
- (56) Irwin, J. J.; Shoichet, B. K. ZINC: A free database of commercially available compounds for virtual screening. *J. Chem. Inf. Model.* **2005**, *45*, 177–182.
- (57) Abdel-Magid, A. R.; Carson, K. G.; Harris, B. D.; Maryanoff, C. A.; Shah, R. D. Reductive amination of aldehydes and ketones with sodium triacetoxyborohydride. Studies on direct and indirect reductive amination procedures. *J. Org. Chem.* **1996**, *61*, 3849–3862.
- (58) Carpino, L. A. 1-Hydroxy-7-azabenzotriazole. An efficient peptide coupling additive. *J. Am. Chem. Soc.* **1993**, *115*, 4397–4398.
- (59) Carpino, L.; El-Faham, A.; Minor, C. A.; Albericio, F. Advantageous applications of azabenzotriazole (triazolopyridine)-based coupling reagents to solid-phase peptide synthesis. *J. Chem. Soc., Chem. Commun.* **1994**, 201–203.
- (60) Carpino, L. A.; El-Faham, A.; Truran, G. A.; Triolo, S. A.; Shroff, H.; Griffin, G. W.; Minor, C. A.; Kates, S. A.; Albericio, F. Azabenzotriazole-based coupling reagents in solid-phase peptide synthesis. In *Peptides: Chemistry, structure and biology: Proceedings of the Thirteenth American Peptide Symposium*; Hodges, R. S., Smith, J. A., Eds.; ESCOM, 1994; pp 124–126.
- (61) Ehrlich, A.; Rothmund, S.; Brudel, M.; Beyermann, M.; Carpino, L. A.; Bienert, M. Synthesis of cyclic peptides via efficient new coupling reagents. *Tetrahedron Lett.* **1993**, *34*, 4781–4784.
- (62) Willstaetter, R.; Pfannenstiel, A. Quinone amines. III. *Ber. Dtsch. Chem. Ges.* **1904**, *37*, 4605–4609.
- (63) Sah, P. P. T.; Brull, W. A rapid and practical process for the preparation of 2-methyl-1-hydroxy-4-aminonaphthalene hydrochloride or vitamin K5 from 2-methyl-1,4-naphthoquinone. *Ber. Dtsch. Chem. Ges.* **1941**, *74B*, 552–554.
- (64) Kalisiak, J.; Sharpless, K. B.; Fokin, V. V. Efficient synthesis of 2-substituted-1,2,3-triazoles. *Org. Lett.* **2008**, *10*, 3171–3174.
- (65) Dogadkin, B. A.; Eitingon, I. I.; Fel'dshtein, M. S.; Tarasova, Z. N.; Gur'anova, E. N.; Lin, Y. T.; Klauzen, N. A.; Pevzner, D. M. Rubber vulcanization in the presence of aminomethyl derivatives of 2-mercaptopbenzothiazole as accelerators. *Kolloidn. Zh.* **1959**, *21*, 427–435.
- (66) Vernin, G.; Siv, C.; Metzger, J. Synthesis and physicochemical study of sulfides, sulfoxides and sulfones in the thiazole series. *J. Heterocycl. Chem.* **1978**, *15*, 1361–1366.
- (67) Kung, A. C.; Falvey, D. E. Photogenerated N-methyl-N-1-naphthylnitrenium ion: Laser flash photolysis, trapping rates, and product study. *J. Org. Chem.* **2005**, *70*, 3127–3132.
- (68) Yamamoto, H.; Maruoka, K. Novel N-alkylation of amines with organocopper reagents. *J. Org. Chem.* **1980**, *45*, 2739–2740.
- (69) Kraus, G. A.; Kim, J. Direct synthesis of 5-substituted naphthoquinones. *J. Org. Chem.* **2002**, *67*, 2358–2360.
- (70) Bunce, N. J.; Cater, S. R.; Scaiano, J. C.; Johnston, L. J. Photo-substitution of 1-methoxy-4-nitronaphthalene with amine nucleophiles: Dual pathways. *J. Org. Chem.* **1987**, *52*, 4214–4223.
- (71) Soroka, J. Photochemistry of hemicyanines IV: Synthesis of (±)-5,6-dihydronaphtho[2,1-c]-quinolizinium salts. *J. Photochem. Photobiol., A* **1992**, *64*, 171–182.
- (72) Knölker, H.; Bauermeister, M.; Pannek, J.; Wolpert, M. Transition metal-diene complexes in organic-synthesis, Part 22. The iron-mediated quinone imine cyclization: A general route to 3-hydroxy-carbazoles. *Synthesis* **1995**, 397–408.
- (73) Röhrig, U.; Grosdidier, A.; Zoete, V.; Michielin, O. Docking to heme proteins. *J. Comput. Chem.* **2009**, *30*, 2305–2315.
- (74) Brooks, B. R.; Brucoleri, R. E.; Olafson, B. D.; States, D. J.; Swaminathan, S.; Karplus, M. CHARMM: A program for macromolecular energy, minimization, and dynamics calculations. *J. Comput. Chem.* **1983**, *4*, 187–217.
- (75) MacKerell, A. D., Jr.; et al. All-atom empirical potential for molecular modeling and dynamics studies of proteins. *J. Phys. Chem. B* **1998**, *102*, 3586–3616.
- (76) Lee, M. S.; Feig, M.; Salisbury, F. R., Jr.; Brooks, C. L., III New analytic approximation to the standard molecular volume definition and its application to generalized born calculations. *J. Comput. Chem.* **2003**, *24*, 1348–1356.
- (77) Stultz, C. M.; Karplus, M. Fragment docking to proteins with the multi-copy simultaneous search methodology. In *Fragment-based Approaches in Drug Discovery*; Jahnke, W., Erlanson, D. A., Eds.; NetLibrary, 2006; pp 125–156.
- (78) Lippert, G.; Hutter, J.; Parrinello, M. A hybrid Gaussian and plane wave density functional scheme. *Mol. Phys.* **1997**, *92*, 477–487.
- (79) VandeVondele, J.; Krack, M.; Mohamed, F.; Parrinello, M.; Chassaing, T.; Hutter, J. Quickstep: Fast and accurate density functional calculations using a mixed Gaussian and plane waves approach. *Comput. Phys. Commun.* **2005**, *167*, 103–128.
- (80) CP2K developers group, CP2K, freely available at <http://cp2k.berlios.de>, released under GPL license **2007**.
- (81) Goedecker, S.; Teter, M.; Hutter, J. Separable dual-space Gaussian pseudopotentials. *Phys. Rev. B* **1996**, *54*, 1703–1710.
- (82) Hartwigsen, C.; Goedecker, S.; Hutter, J. Relativistic separable dual-space Gaussian pseudopotentials from H to Rn. *Phys. Rev. B* **1998**, *58*, 3641–3662.
- (83) Perdew, J.; Burke, K.; Ernzerhof, M. Generalized gradient approximation made simple. *Phys. Rev. Lett.* **1996**, *77*, 3865–3868.
- (84) Liu, D. C.; Nocedal, J. On the limited memory BFGS method for large scale optimization. *Math. Programming* **1989**, *45*, 503–528.
- (85) Blöchl, P. E. Electrostatic decoupling of periodic images of plane-wave-expanded densities and derived point charges. *J. Chem. Phys.* **1995**, *103*, 7422–7428.
- (86) Rovira, C.; Carloni, P.; Parrinello, M. The iron-sulfur bond in cytochrome C. *J. Phys. Chem. B* **1999**, *103*, 7031–7035.
- (87) Takikawa, O.; Kuroiwa, T.; Yamazaki, F.; Kido, R. Mechanism of interferon- γ action. Characterization of indoleamine 2,3-dioxygenase in cultured human cells induced by interferon- γ and evaluation of the enzyme-mediated tryptophan degradation in its anticellular activity. *J. Biol. Chem.* **1988**, *263*, 2041–2048.
- (88) Austin, C. J. D.; Astelbauer, E.; Kosim-Satyaputra, P.; Ball, H. J.; Willows, R. D.; Jamie, J. E.; Hunt, N. H. Mouse and human indoleamine 2,3-dioxygenase display some distinct biochemical and structural properties. *Amino Acids* **2009**, *36*, 99–106.
- (89) Dick, R.; Murray, B. P.; Reid, M. J.; Correia, M. A. Structure-function relationships of rat hepatic tryptophan 2,3-dioxygenase: Identification of the putative heme-ligating histidine residues. *Arch. Biochem. Biophys.* **2001**, *392*, 71–78.
- (90) Pettersen, E. E.; Goddard, T.; Huang, C.; Couch, G.; Greenblatt, D.; Meng, E.; Ferrin, T. E. UCSF Chimera: A visualization system for exploratory research and analysis. *J. Comput. Chem.* **2004**, *25*, 1605–1612.
- (91) Morris, G. M.; Goodsell, D.; Halliday, R.; Huey, R.; Hart, W. E.; Belew, R. K.; Olson, A. J. Automated docking using a Lamarckian genetic algorithm and an empirical binding free energy function. *J. Comput. Chem.* **1998**, *19*, 1639–1662.